Title

CHAPTER 9 Bijels the Easy Way

ISBN

9781788015202

Authors

Forth, Joe

Toor, Anju

Chai, Yu

et al.

Publication Date

2020

DOI

10.1039/9781839160974-00211

Peer reviewed

ChapTer 9

Bijels the Easy Way

Joe ForTh[a,b], anJu Toor[a,c], Yu Chai[a,c,d], Caili huang[a,e], Xubo liu[a,f], Wenqian Feng[a,g], ShaoWei Shi[f], Dong Wang[f], paul D. aShbY[a,d], breTT a. helmS[a,d] anD ThomaS p. ruSSell*[a,f,h,i]

[a]materials Sciences Division, lawrence berkeley national laboratory, berkeley, Ca 94720, uSa; [b]Department of Chemistry, university College london, london, WC1h 0aJ, uK; [c]School of materials Science and engineering, university of California, berkeley, Ca 94720, uSa; [d]The molecular Foundry, lawrence berkeley national laboratory, berkeley, Ca 94720, uSa; [e]Key laboratory of material Chemistry for energy Conversion and Storage, ministry of education, School of Chemistry and Chemical engineering, huazhong university of Science and Technology, Wuhan, 430074, China; [f]beijing advanced innovation Center for Soft matter Science and engineering, beijing university of Chemical Technology, beijing 100029, China; [g]max planck institute for medical research, 69120 heidelberg, germany; [h]advanced institute for materials research (Wpi-aimr), Tohoku university, aoba, Sendai 980-8577, Japan; [i]polymer Science and engineering Department, university of massachusetts, Conte Center for polymer research, massachusetts, 01003, uSa
*e-mail: russell@mail.pse.umass.edu

9.1 Introduction

The overwhelming majority of this book focuses on bicontinuous interfa- cially jammed emulsion gels (‘bijels’) that are formed *via* spinodal decom- position.[1,2] This strategy for forming bijels has a number of compelling

advantages (Chapter 1). if well controlled, it can lead to liquid bicontinuous systems with domains that percolate on macroscopic length scales (centi- metres or more), with a single, well-defined, controllable channel width of 1 mm or less, potentially as low as 1 μm.[3,4] The structures generated by spinodal decomposition are also potentially useful in many applications such as chemical synthesis and separations, while the zero mean curvature of the bijels make them resistant to ostwald ripening. if a suitably homogeneous quench can be achieved, significant sample volumes (of the order of millilitres) of bijel can be produced in a process that, while not truly scalable, brings bijels into the realms of high-added-value applications (Chapter 2). Furthermore, producing bijels *via* spinodal decomposition, in which a three-dimensional (3D) structured liquid system is formed by the jamming of a two-dimensional (2D) particle assembly, is *elegant* – a quality that should not be dismissed.

using spinodal decomposition to form bijels does, however, have a num- ber of disadvantages. The biggest challenge faced when producing a bijel is in producing colloidal particles that wet the two liquid phases equally.[5] While there has been some success in bypassing this challenge by using mixtures of particles with well-characterized contact angles,[6] achieving finely tuned particle wetting remains a significant challenge. The second difficulty lies in evenly quenching the system to achieve demixing of the two liquids. Traditionally, bijels were quenched into the spinodal region of the liquid–liquid phase diagram using a rapid change in temperature. Changes in temperature are, however, notoriously difficult to work with, especially in liquids, where temperature gradients drive convection, and in which generation of a temperature change without a spatial tempera- ture gradient is effectively impossible to achieve. production of bijels *via* solvent transfer-induced phase separation (STripS), which uses a chemical quench instead (Chapter 6), is a compelling strategy for producing bijels without using an experimentally delicate parameter, such as temperature or pressure.[7–11] This method also has the added benefit that it produces bijel threads in a geometry suitable for a number of industrial applications built around flow-through of liquids, such as chemical synthesis. however, STripS bijels contain fibres with liquid domains of multiple length scales. Furthermore, regardless of how the temperature quench is applied or how particle wetting is manipulated, the resulting geometry of the bijels pro- duced *via* spinodal decomposition makes it extremely challenging to fully exploit some of the more interesting functional properties of liquid–liquid interfaces at which particles, particularly nanoparticles, are adsorbed.[12,13] in the last decade, we have worked to develop methods to produce liquid bicontinuous structures using interfacial jamming of particles without using spinodal decomposition.

all interfacially structured liquids, be they foams,[14,15] emulsions,[16–18] liquid marbles,[19,20] or bijels,[21,22] are built using the same principle. First, one liquid is pre-formed inside a second, immiscible liquid

üśing a range of methods, such as the application of shear stress or demixing. Surface-active

material must then adsorb onto the liquid–liquid interface, arresting hydro- dynamic instabilities and guiding the system through a kinetic trajectory that produces the desired morphology. Surface tension between the two immiscible liquids causes the amount of interfacial area to decrease with time, increasing the areal density of adsorbed matter. if the interfacially adsorbed material is irreversibly bound to the liquid–fluid interface, this reduction in surface area will eventually cause the particle assembly to jam into a solid-like, load-bearing material that can support anisotropic surface stresses.

in this chapter, we look at how these physical principles can be applied to produce liquid bicontinuous systems, often with functionally useful, stimulus–responsive interfaces, with properties that are not readily acces- sible to systems produced using spinodal decomposition. We begin by discussing a rather general mechanism for forming solid-like nanopar- ticle assemblies at the oil–water interface with effectively arbitrary func- tionality. The bulk of this chapter is then dedicated to the recent work performed by us, and others, in harnessing hydrodynamics and solidify- ing interfacial assemblies to structure liquids into complex shapes, thus forming bijels in a wealth of different ways. We show how jamming of the nanoparticle surfactant assemblies kinetically traps systems of immis- cible liquids in non-equilibrium shapes indefinitely, while the liquids retain all their desirable characteristics, for example, mobility, and mass transport.[6,23–26] Finally, we discuss the applications of these systems in chemical separations, chemical synthesis with heterogeneous catalysis and inline purification, and all-liquid actuators.

9.2 Nanoparticle Surfactants: A Model System for the Rapid Assembly of Solid-like Interfaces

nanoparticles (nps) exhibit a wide range of interesting physical and func- tional traits, such as tunable optical properties,[12,27] electronic conductiv- ity,[28] and ferromagnetism.[29,30] at the same time, the assembly of nps at the liquid–liquid interface provides an attractive platform to produce arrays of nps with bespoke functional properties, which derive from both the nps and their dimensional confinement.[31,32] Furthermore, if the particles can be bound strongly enough to the oil–water interface, they can also be used to structure liquids into complex shapes.[23,25] Combining all three of these factors can, however, be rather difficult. nanoparticle surfac- tants (npS), which consist of polymer surfactants dispersed in one phase and nanoparticles dispersed in a second, immiscible phase (Figure 9.1), provide us with an easy-to-use strategy to achieve this. provided that the nanoparticles and surfactants contain complementary functional groups (*e.g.*, $-nh_2$ and –Cooh) the nps and

polymers interact with one another at the liquid–liquid interface to form npS: asymmetric, polymer- nanoparticle composites that are irreversibly adsorbed to the oil–water

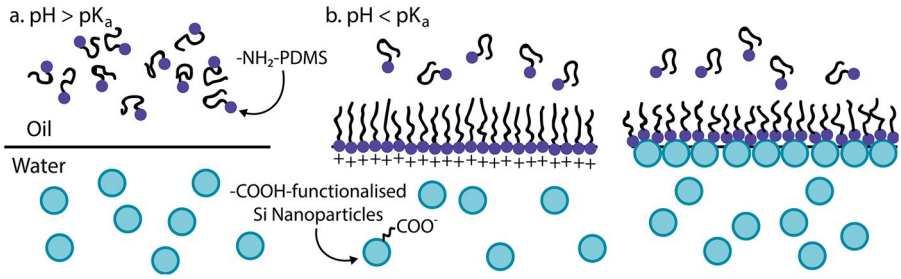

Figure 9.1 assembly of nanoparticle surfactants at the oil–water interface. (a) polymer surfactants and non-adsorbing nanoparticles bearing com- plementary functional groups (in this case –nh$_2$ and –Cooh) are ini- tially dispersed in separate, immiscible liquids. (b) below a critical ph the amine group protonates and adsorbs to the oil–water inter- face. electrostatic interactions between the polymer and the surface groups of the particles drive adsorption of the particles to the oil– water interface.

interface. in the case of polymers bearing –nh$_2$ groups and nanoparti- cles bearing –Cooh groups, at ph values at or below the pK_a of the –nh$_2$ group, the amine protonates and adsorbs to the oil–water interface.[33,34] This positively charged amine monolayer drives the adsorption of the nanoparticles to the oil–water interface, forming a monolayer of Janus nanoparticle surfactants that is irreversibly adsorbed to the oil–water interface, even when using nps that would not otherwise adsorb to the interface (Figure 9.1b).

npS have a number of advantages over the micrometre-sized colloi- dal particles typically used to stabilize bijels. First, electrostatic interac- tions between the nanoparticles and surfactants result in extremely rapid adsorption of particles to the interface, relative to what would be expected purely from diffusion.[35] Second, nanometre-sized nanoparticles with homogeneous surface chemistry have adsorption energies of the order of kT, and readily exchange with nanoparticles in the bulk, meaning that they cannot stabilize non-spherical droplets.[36] nanoparticle surfactants, however, consist of an extremely hydrophobic moiety attached to the sur- factant and a highly polar nanoparticle, rendering them strongly bound to the liquid–liquid interface.[23] perhaps most importantly, interfacial adsorption of npS requires only that the functional groups of the polymer and particles are complementary, bypassing the need for painstaking tuning of the surface chemistry of the particles. as such, even nanopar- ticles that do not typically adsorb to the oil–water interface can be used to form irreversibly adsorbed, two-dimensional assemblies (Chapter 7). Since the first systematic studies by Cui *et al.*,[23] an immense range of nanoparticles, including graphene oxide,[37] single-walled carbon nano- tubes,[38] ligand-stripped Fe_3o_4 nanocrystals,[39] polyoxometalates,[40] as well

as silica and polystyrene nanoparticles, have been used to form stimulus- responsive, interfacial assemblies that can shape liquids into complex structures.[25]

The driving force behind the assembly of large populations of npS (and, indeed, most materials) at the oil–water interface is the reduction in the sur- face tension, γ, between the two liquids. most intuitively, γ is the free energy cost, G, per unit area, A, associated with the existence of a liquid–liquid inter- face, and can be defined both as the ratio of these quantities and in terms of the corresponding partial derivative:[22]

$$\gamma \equiv \frac{G_\gamma}{A} \tag{9.1}$$

$$\gamma = \left(\frac{\partial G}{\partial A}\right)_{T,V} \tag{9.2}$$

less intuitively, but importantly for liquid–fluid interfaces at which mate- rial is irreversibly adsorbed, γ can also be described in terms of a force per unit length of interface that acts *tangentially* to the interface. a number of excellent articles exist to describe this physically non-intuitive idea.[41–43]

adsorption of material to the oil–water interface typically reduces γ by screening energetically expensive interactions between the two immiscible solvents (although we note that the finer points of this, in the case of col- loidal particles, remains a subject of some controversy).[44] The reduction in interfacial energy associated with the adsorption of a nanoparticle of radius, r, to the oil–water interface is given by:

$$\Delta G_\gamma = \pi r^2 \gamma \left(1 - \left|\frac{\gamma_{op} - \gamma_{wp}}{\gamma_{ow}}\right|\right)^2 \tag{9.3}$$

where γ_{op}, γ_{wp}, and γ_{ow} are the oil–particle, water–particle, and oil–water inter- facial tensions respectively. if ΔG_γ is sufficiently large (of the order of 100 kT, although this figure is a matter of open study)[45–47] then the particles are effectively irreversibly trapped at the interface.

There is a thermodynamic drive for the system to reduce the total amount of oil–water interface in the system, causing droplets of one liquid inside another liquid to be spherical. Very generally, the presence of any curved interface (be it spherical or otherwise) is associated with a pressure differ- ence, ΔP, between the internal and external phases. The principal radii of curvature, κ_1 and κ_2, in such systems are related to this pressure difference by a surface stress tensor, $\boldsymbol{\sigma}_s$, giving the generalised Young–Laplace equation:[48]

$$\Delta P = \kappa_1 \sigma_{11} + \kappa_2 \sigma_{22} \tag{9.4}$$

at low areal particle densities, or for reversible particle

attachment, adsorption of particles to the liquid–fluid interface simply acts to reduce the

surface tension. in the case of reversibly adsorbed particles, the shape of the liquid–liquid interface is well described by the special case of eqn (9.4) where $\kappa_1 = \kappa_2$ and $\boldsymbol{\sigma}$s = γ, and γ is a scalar, *i.e.*,

$$\Delta P = \frac{2\gamma_{ow}}{R} \tag{9.5}$$

liquid–liquid interfaces in this case are either spherical or flat, depending on the density differences between the two fluids. as the interface is com- pressed, interactions between the particles become significant. if the par- ticles are irreversibly adsorbed to the liquid–liquid interface, they jam or solidify into a load-bearing structure and a scalar γ is no longer appropriate to describe the stresses acting on the interface; these stresses must now be described using the full 2 × 2 surface stress tensor. hermans *et al.* applied this concept to heuristically break the stresses acting on a liquid–fluid inter- face into two distinct origins:[49]

$$\boldsymbol{\sigma}_s = \gamma\delta_{ij} + \boldsymbol{\Gamma}_{ij} \tag{9.6}$$

where δ_{ij} is the Kronecker delta. here, γ is an isotropic, scalar quantity corresponding to the free energy cost per unit area associated with deform- ing the liquid–fluid interface itself, while $\boldsymbol{\Gamma}_{ij}$ is an anisotropic, tensor quan- tity that is derived from the mechanical properties of the adsorbed layer of material. intuitively, eqn (9.6) states that when we deform a liquid–fluid interface at which a material has been formed or adsorbed, we must do work to deform both the liquid–fluid interface and the material that is adsorbed at the interface. enormous progress has been made in under- standing the rheology and mechanical properties of complex interfaces in recent years,[50] most significantly from Vermant and Fuller and co-workers from an experimental perspective,[51–53] and from Sagis on the theoretical side.[54,55] The underlying theory is rather involved and not covered here, however, the phenomenology that solid and jammed interfacial assemblies lead to is quite intuitive.

nanoparticle surfactants provide a striking example of the phenomena that are characteristic of irreversibly adsorbed particle monolayers (Figure 9.2). placing an aqueous droplet of Cooh-functionalized nanoparticles in a bath of high-viscosity silicone oil that contains polydimethoxysilox- ane (pDmS)-nh_2 leads to the formation of npS at the oil–water interface (Figure 9.2a). applying an external electric field to the system deforms the droplet due to the difference in the dielectric constants of the two media. This deformation leads to the formation of more interfacial area and, therefore, more npS. Switching off the field leads to contraction of the interface to minimize G_γ. however, as the interface contracts, the npS jam, and $\boldsymbol{\Gamma}_{ij}$ becomes significant, thus preventing the droplet from relax- ing to a spherical shape and kinetically trapping the droplet in a non- equilibrium shape (Figure 9.2b). Throughout this chapter, we will show

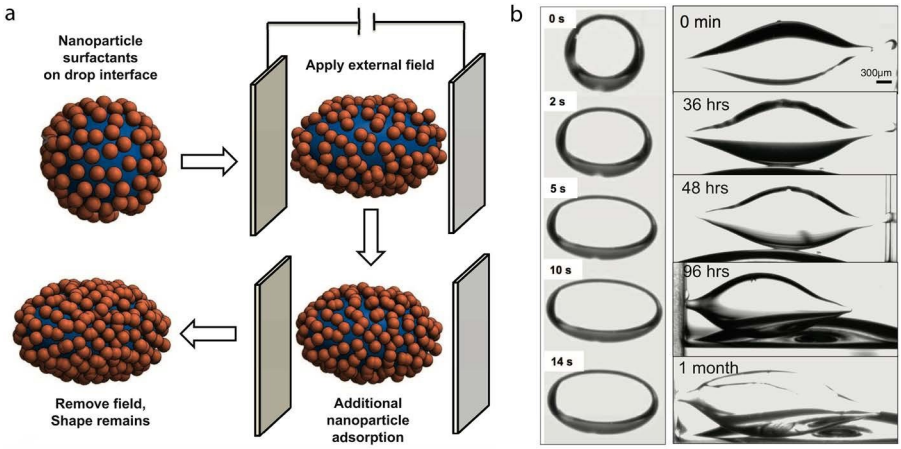

Figure 9.2 using interfacial jamming of nanoparticle surfactant assemblies to kinetically trap water droplets in non-equilibrium shapes. (a) Sche- matic and (b) implementation of non-equilibrium drop-shape gen- eration. npS first assemble at an undeformed oil–water interface. Deformation of a water droplet in oil using an electric field causes more npS to assemble at the interface. When the electric field is switched off, the droplet tends to minimize the oil–water surface area and adopt a spherical shape but is prevented from doing so by the jamming of the assembled npS. reproduced from ref. 23 with per- mission from american association for the advancement of Science, Copyright 2013.

how this jamming of an interfacial assembly of nanoparticles can arrest hydrodynamic instabilities, enabling us to produce reconfigurable, liquid bicontinuous systems with highly controlled structural and functional properties.

9.3 Arresting Plateau–Rayleigh Instabilities With Interfacial Jamming

To produce long-lasting, liquid bicontinuous structures it is necessary to assemble a jammed npS film that arrests plateau–rayleigh (pr) instabili- ties indefinitely. To do this, two things must be achieved. First, a cylindri- cal tube of water must be formed in the oil phase. in high-viscosity oils, this is achieved by dragging the print head from which the aqueous phase emerges through the oil sufficiently quickly so that viscous stresses over- come surface tension.[56] in low-viscosity oils it is done by using either sufficiently high flow rates or by achieving sufficiently low surface tensions, such that the inertia of the water emerging from the print head over- comes surface tension, leading to the formation of an unstable aqueous

cylinder.[26,57] Second, the npS assembly must solidify or jam more rapidly than the liquid jet breaks up into droplets. The timescale of break-up, τ, of a cylinder of one viscous liquid inside another is given by:

$$\tau = \alpha \frac{\eta d}{\gamma} \tag{9.7}$$

where η is the viscosity of the external liquid, d is the diameter of the cylinder, γ is the liquid–liquid surface tension, and α is a numerical factor between approximately 10 and 100, which is determined by the viscosity difference between the two liquids.[58–60] in practice, for the tubules of interest in this work d = 10–1000 μm, $\gamma \approx$ 0.1–20 mn m^{-1}, and η = 0.5–10 000 mpa s. The timescale of break-up, τ, can be varied between 10^{-3} and 10^{2} s by changing any of these parameters. arresting the break-up of 1 mm diameter tubules in a low-viscosity water–toluene system ($\gamma \approx$ 10 mn m^{-1}, η = 0.5 mpa s, $\alpha \approx$ 50) requires the npS to assemble and jam within approximately 25 ms.

liu *et al.* achieved this by using rod-like cellulose nanocrystal (CnC)- based npS, termed CnC surfactants (CnCS), which form very rapidly at the liquid–liquid interface.[61] an important characteristic of CnCs prepared by a sulfuric acid hydrolysis is that sulfate half-esters (–oSo^{3-}) are grafted onto the surface of the crystallites, which prevent aggregation of the CnCs in aqueous dispersions.[62] For the purpose of forming liquid tubules, these charged groups also provide anchoring points for polymer chains for the interfacial formation of CnC surfactants. by adjusting the ph, concentra- tions of the CnC and end-functionalized polymer, and flow conditions, the dripping-to-jetting transition can be achieved easily due to the significantly reduced interfacial energy and the resultant aqueous tubules can be effec- tively stabilized indefinitely by the interfacial assembly and jamming of CnC surfactants (Figure 9.3).

liu *et al.* initially investigated how CnCS assembly rates and density could be controlled by varying polymer molecular weight and concen- tration.[61] The dynamic interfacial tension reduction for different molec- ular weights of amine-functionalized polystyrene (pS-nh$_2$, M_w = 1500, 2500, 13 000, 25 000, and 40 000 g mol^{-1}) was studied at ph 3 (Figure 9.4a, [CnC] = 10 mg ml^{-1}, [pS-nh$_2$] = 1 mg ml^{-1}). lower molecular weights of pS-nh$_2$ led to lower interfacial tensions. The pS-nh$_2$ of M_w = 1500 g mol^{-1} showed the strongest interfacial activity and reached a constant surface tension rapidly. Similar behaviour was observed for pS-nh$_2$ with M_w = 2500 g mol^{-1}, but with a higher equilibrium γ of approximately 10 mn m^{-1}. For M_w = 13 000 g mol^{-1}, the decrease in γ is much slower in comparison to that for 1500 g mol^{-1} and 2500 g mol^{-1} due to the lower diffusion coefficient of the larger molecule. pS-nh$_2$ with M_w = 25 000 g mol^{-1} and 40 000 g mol^{-1} show almost no interfacial activity. lower interfacial tensions were found to be

directly linked to a higher density of particles at the oil–water inter- face. CnCS assembled using a lower molecular weight polymer surfactant yielded pendant drops with a lower surface tension, and these droplets

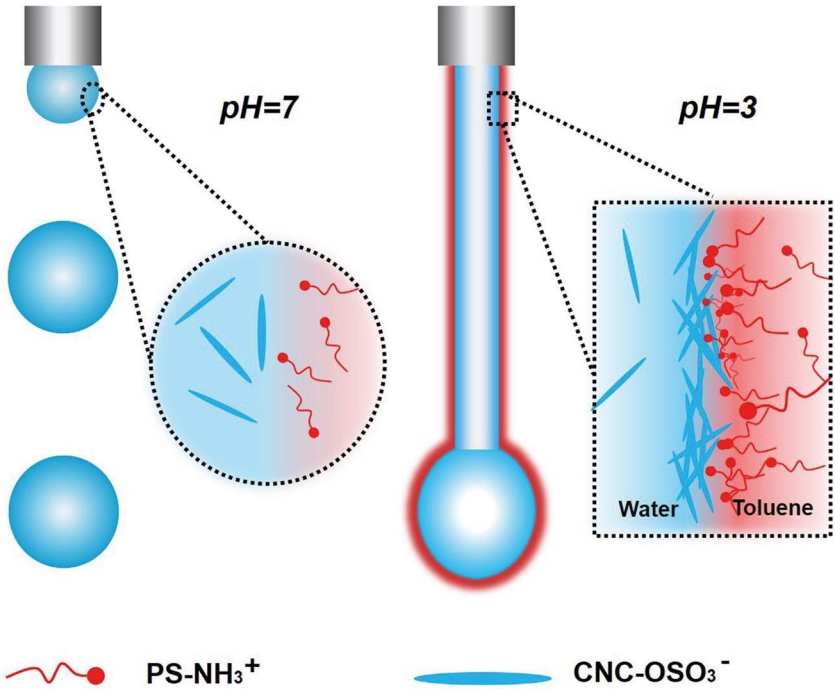

Figure 9.3 Schematic illustration of kinetically trapping a liquid jet in a tubular shape through the ph-dependent assembly and jamming of CnC sur- factants at the water–toluene interface. reproduced from ref. 61 with permission from John Wiley and Sons, © 2017 Wiley-VCh Verlag gmbh & Co. Kgaa, Weinheim.

buckled at lower compressions, indicative of a higher real particle den- sity. This was in strong contrast to CnCS assembled using high molecular weight polymer surfactants, which produced pendant drops that exhibited buckling only at large compressions (Figure 9.4b).

The effect of CnC surfactants on pr instabilities of water jets was then investigated using a pendant drop tensiometer in a constant flow mode, which injects aqueous CnC dispersions into toluene solutions of polymer ligands through a narrow capillary at a constant rate (Figure 9.5). as dis- cussed above, ph plays a key role in determining the interfacial activity of the CnC surfactants. Figure 9.5a shows the break-up of the water jet in tolu- ene at different ph values. The concentrations of both the CnC and pS-nh_2 were fixed at 10 mg ml^{-1}, the molecular weight of the pS-nh_2 is 1500 g mol^{-1}, and the capillary diameter is 0.5 mm. With a flow rate of 1.5 ml min^{-1}, a dripping-to-jetting transition is clear, with decrease in the ph from 7.45 to
2. For ph values of 5.03 and 7.45, droplets are formed periodically at the ori- fice of the capillary and no jetting is observed, which is characteristic of the dripping break-up mode (Figure 9.5a).[63] at the base of the cell the spherical droplets coalesce and fuse into a larger pool of the aqueous

phase, indicating

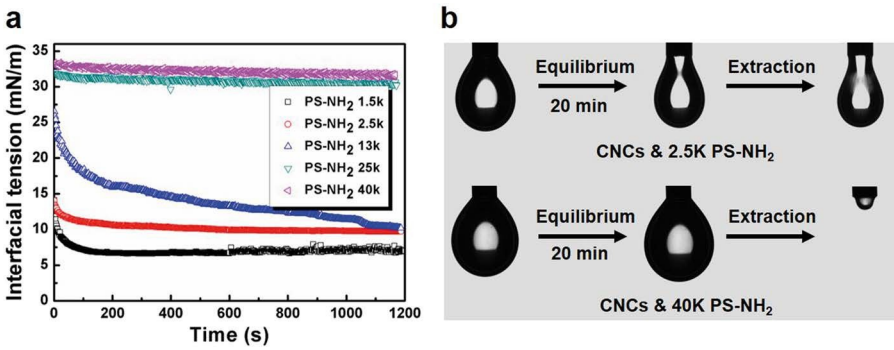

Figure 9.4 The effect of polymer surfactant concentration and molecular weight upon CnCS assembly and interfacial tension. (a) Time evolution of interfacial tension of the water–toluene interface at which CnCS are assembling with different pS-nh$_2$ molecular weights (ph = 3). (b) buck- ling behavior of the droplet surface after the system has reached a con- stant surface tension (after 20 min). The concentrations of CnC and pS-nh$_2$ in water and toluene are 10 mg ml^{-1} and 1 mg ml^{-1}, respec- tively. adapted from ref. 61 with permission from John Wiley and Sons,

that the CnC surfactants assembled on the surface of the droplets are not jammed. This behaviour is similar to that seen with a pure water droplet in toluene. This result is consistent with the rate of reduction in the interfacial tension, where the rate of CnC surfactant formation and assembly in this high-γ region is low.

When the ph is decreased to 3.72, tadpole-like structures are formed, with spherical 'heads' and tubular 'tails'. These non-equilibrium shapes are stabilized by the interfacial jamming of CnC surfactants and no coales- cence of the structured liquids occurs at the base of the cells. Figure 9.5b and c shows sequential images captured during the break-up of the water jet using a high frame rate of 5400 fps, with CnC/pS-nh$_2$ concentrations of 10/10 mg ml^{-1} and 0/10 mg ml^{-1}, respectively (ph = 3). The formation of tadpole-like drops, in which pr instabilities are partially arrested in the liquid cylinder can be seen, and no satellite droplets form (Figure 9.5b). initially, as the aqueous phase is injected into the toluene solution, a droplet forms and grows in size at a rate dictated by the rate of injec- tion of the aqueous phase. The reduction in the interfacial tension causes the droplet to assume a slightly elongated shape. as more aqueous phase is injected, the total mass of the droplet increases, and a combination of gravitational forces and low surface tension causes the droplet to fall and form a tubular structure. eventually, the rate at which free surface is generated becomes greater than the rate at which the np surfactants can form, assemble, and jam, and the droplet with the trailing tubule breaks off. The arrested tubular shapes show elastic properties and contract after the separation to decrease the interfacial area, then jam, retaining the

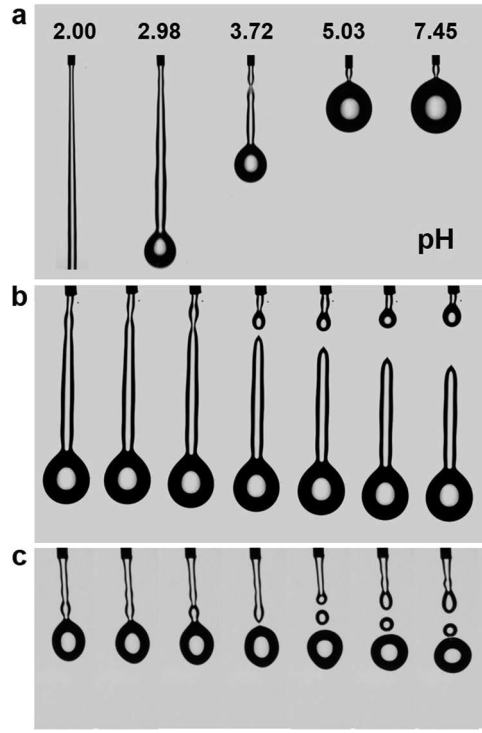

Figure 9.5 effect of ph upon CnC surfactant assembly and jetting and dripping modes. (a) break-up length variation of an aqueous CnC solution (10 mg ml^{-1}) injected into toluene solution containing pS-nh_2 (10 mg ml^{-1}) with different ph. (b) an aqueous CnC solution (10 mg ml^{-1}, ph = 3) falling in a toluene solution containing pS-nh_2 (10 mg ml^{-1}). The interval between consecutive images is 4 ms. (c) Water (ph = 3) injected into toluene containing pS-nh_2 (10 mg ml^{-1}). The interval between consecutive images is 4 ms. reproduced from ref. 61 with permission from John Wiley and Sons, © 2017 Wiley-VCh Verlag gmbh & Co. Kgaa, Weinheim.

tadpole-like shape. at the base of the cell, the aqueous phase with the tadpole-like structure accumulates, without coalescence. Without CnCs, water droplets injected into a pS-nh_2 solution in toluene (10 mg ml^{-1}) show classic pr instability behaviour with the formation of satellite drop- lets (Figure 9.5c).

With decreasing ph from 3.72 to 2.98, the rate of formation and assembly of the np surfactants increases and the tubule length trailing the droplet increases, as expected. if the ph is decreased further to 2, the break-off of the tubule is completely suppressed, no break-off occurs, and stable tubule gen- eration is observed, with the tubule extending from the needle to the base of the cell. it should be noted that the height of the cell limits the extent to which gravitational forces can contribute, since the tubule rests at the base of the cell, and there is no driving force to break off. This is shown for a system

where the ph is 2.98. When the distance between the nozzle and the sub- strate is shorter than the break-off length, a continuous tubule is observed. When this distance is increased, break-off is again observed.

9.4 3D Printing Water

The work of liu *et al.* showed that by using materials that adsorb extremely rapidly to the interface (such as cellulose nanocrystal surfactants), plateau– rayleigh instabilities can be arrested entirely by interfacial jamming, leading to the formation of long-lasting, millimetre-sized metastable aqueous fibrils in oil. however, very little control could be achieved over the resulting struc- tures, and none of the materials mentioned thus far harness the reconfigu- rability of the npS.

Forth *et al.* made major progress in this area by 3D printing one fluid in another, producing fibrils of water in high-viscosity silicone oil (viscosity, $\eta > 10\ 000$ cSt).[64] The production of threads in the viscous oil uses a slightly different physical principle than the inertial jetting of liu and co-workers. by dragging a needle through the oil at a velocity, v, viscous stresses act to distort the shape of the droplet as it emerges from the capillary. The bal- ance of viscous and surface stresses in the system is given by the capillary number, Ca:

$$Ca = \frac{\eta v}{\gamma} \quad \frac{\text{Viscous Stresses}}{\text{Surface Tension}} \tag{9.8}$$

For Ca ≳ 5, viscous stresses overcome surface tension and extruded water is dragged into a cylindrical thread. Combining this principle with the nanoparticle surfactant system of Cui *et al.*, it was shown that, by connecting a syringe pump to a $350 3D printer, complex, three-dimensional structures of aqueous fibrils in oil could be produced (Figure 9.6). Successful printing of water in oil was readily achieved using particle concentrations as low as 1 mg ml^{-1} and polymer surfactant concentrations of 5% w/w. buffering the aqueous phase using 5 mm 2-(*N*-morpholino)ethanesulfonic acid (meS) and adjusting the ph to 6.4 (significantly below the pK_a of the amine group, close to the pK_a of the meS buffer) resulted in more rapid assembly of the npS and higher quality prints.

using a 3D printer allows a wide variety of structures to be made (Figure 9.7) and no upper limit of print size was observed, with prints up to 1 m in length having been produced. printing in low-viscosity oil pro- duces threads of approximately the same diameter as the print head. in contrast, as observed by utada *et al.*,[56,65] using a high-viscosity liquid as the external medium leads to a 'self-flow-focusing' effect, where threads several orders of magnitude smaller than the print head can be produced. This allows threads with diameters between 10 μm and 1 mm to be pro- duced just by using a 14-gauge needle (internal diameter ≈ 1.4 mm) and varying the flow rate of the aqueous phase or the

translational velocity of the print head. nanoparticles of arbitrary composition can be used with

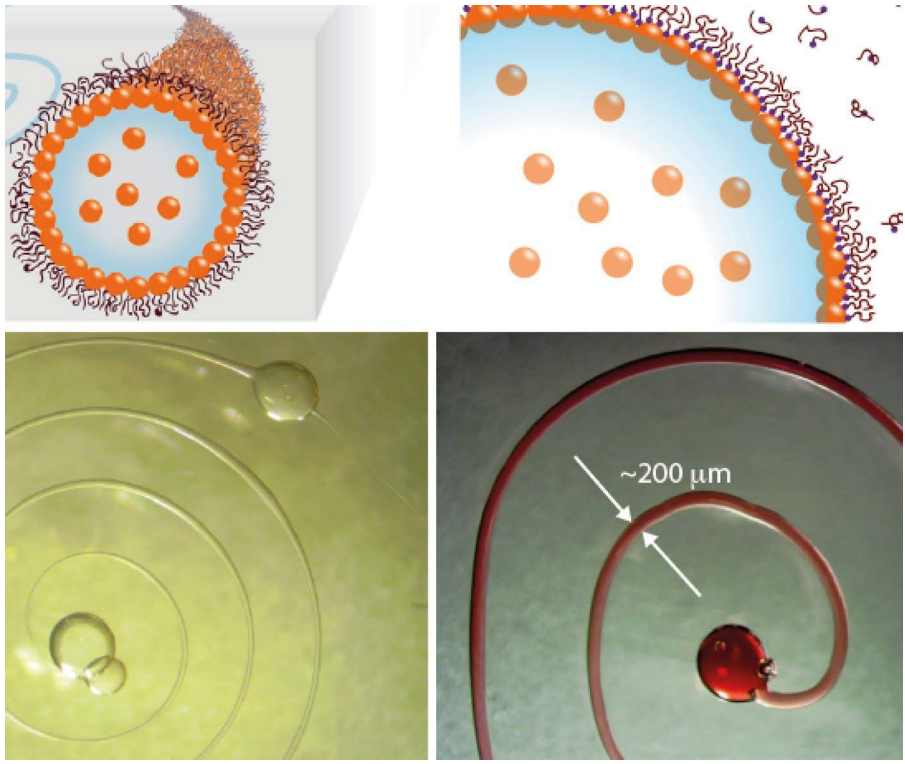

Figure 9.6 3D printed water. (Top, left) Schematic of the production of 3D printed aqueous threads in high-viscosity silicone oil. (Top, right) Schematic showing the stabilization of the printed liquid threads due to the inter- facial assembly and jamming nanoparticle surfactants. (bottom, left) an aqueous spiral, fibril diameter 100 µm, printed in high-viscosity (60 000 cSt) silicone oil, stabilized by silica nanoparticle surfactants. (bottom, right) an aqueous spiral, fibril diameter 200 µm, stabilized by gold nanoparticle surfactants. all scale bars, 2 mm. reproduced from ref. 64 with permission from John Wiley and Sons, © 2018 WileY-VCh Verlag gmbh & Co. Kgaa, Weinheim.

this printing technique; both gold npS (Figure 9.6 (bottom, right), note the red colour due to plasmonic effects in the au nps) and cellulose nanocrys- tal surfactants were found to yield high-quality prints. CnC-based prints were found to be particularly robust, making the production of branched pathways, suitable for use in all-liquid microfluidics circuits, trivial (Fig- ure 9.7c). Fully three-dimensional structures could be produced, affording a strategy for the rapid, lithography-free production of three-dimensional microfluidic circuitry (Figure 9.7d). The density difference between the aqueous and non-aqueous phases used in this work was approximately 20 kg m^{-3}. as such, when printed in the liquid phase, the three-dimensional patterns slowly sediment at a rate of 1 mm h^{-1}. as will be seen later, this is sufficiently slow that the system can still be used for all-liquid microfluidics

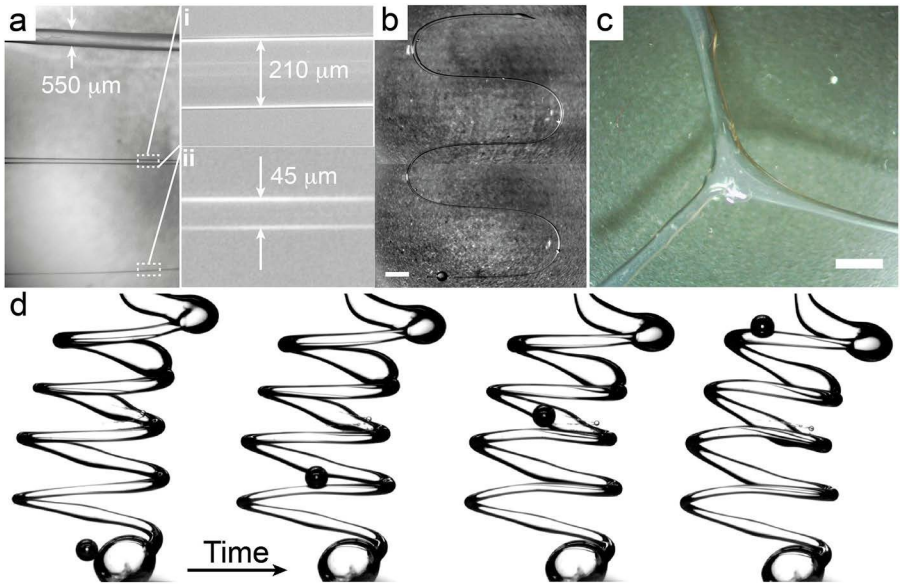

Figure 9.7 Structural diversity achievable with current liquid 3D printing meth- ods. (a) Threads of varying thickness, all printed using the same print head (a 14-gauge needle). (b) extended serpentine paths can be pro- duced with no observed upper limit on length. (c) branched structures of water in oil produced additively. (d) a printed aqueous coil in water slowly sediments. note the air bubble rapidly rising through the cen- tre of the coil. (a, b) 1 mg ml^{-1} silica nanoparticle surfactants, 7.5% w/w pDmS-nh_2. (c) 1 mg ml^{-1} cellulose nanocrystal surfactants, 7.5% w/w pDmS-nh_2. (d) 5 mg ml^{-1} silica nanoparticle surfactants, 7.5% w/w pDmS-nh_2. all scale bars, 2 mm. adapted from ref. 64 with permis- sion from John Wiley and Sons, © 2018 WileY-VCh Verlag gmbh & Co. Kgaa, Weinheim.

applications. While this sedimentation could be stopped trivially by den- sity matching the solvents (if desired), it is interesting to note that, in micro-gravitational conditional conditions (*i.e.*, space), these constructs would be stable indefinitely, making them interesting platforms for space station-based experiments. long-term stability can readily be imparted to the system by using photopolymerisable pDmS as the continuous phase and curing the non-aqueous phase after printing.

9.5 Moulded Water

Shi *et al.*, inspired by the extremely rapid assembly of CnCS at the oil– water interface, moved away from jetting and dragging water, and instead developed a technique to mould water in oil, which they refer to as 'all- liquid moulding'.[66] as with the other techniques so far, liquid moulding employs nps dispersed in one liquid and polymers with complementary

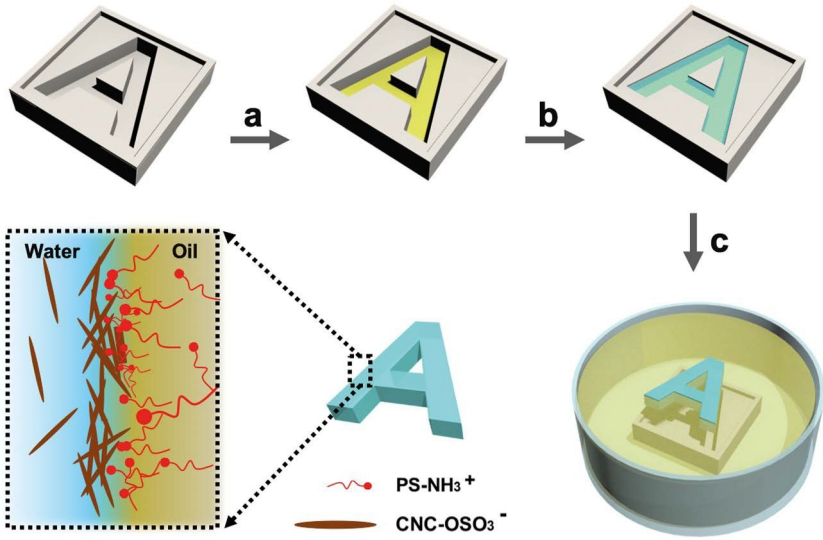

Figure 9.8 Schematic of the all-liquid moulding process. (a) a 3D printed pla mould is initially filled with approximately 100 µl CCl_4 containing pS- nh_2. (b) approximately 200 µl CnC aqueous solution is then gently pipetted on top of the CCl_4. (c) immersing the mould into 10 ml CCl_4 containing pS-nh_2. [pS-nh_2] = 10 mg ml^{-1}, [CnC] = 10 mg ml^{-1}, M_w (pS–nh_2) = 1000 g mol^{-1}. reproduced from ref. 66 with permission from John Wiley and Sons, © 2018 WileY-VCh Verlag gmbh & Co. Kgaa, Weinheim.

functional groups dissolved in a second, immiscible liquid, resulting in the formation and assembly of npS at the liquid–liquid interface. Jamming of the npS at the interface occurs when a compressive force is placed on the npS assemblies, as the system reduces the interfacial area to minimize the interfacial energy.[19] as well as producing extremely robust, jammed interfaces, the CnCs make for interesting ph-dependent viscosity modifiers and structuring agents of the aqueous phase, and so the rheology of the CnC dispersion can range from that of a liquid to that of a cross-linked gel.

liquid moulding works by placing an aqueous dispersion of CnCs of the appropriate ph in a 3D printed pla (polylactic acid) mould (Figure 9.8). much like in traditional moulding, a release agent is required to ensure release of the aqueous phase from the mould. in this case, the ‘release agent’ consisted of pre-wetting the base and walls of the mould with an appropriate amount of ligand, which prevented the CnC solution from sticking to the corners of the cavity. after application of the release agent, a dyed aqueous CnC dispersion was placed on top of CCl_4 solution to fill the mould. The mould containing the dyed aqueous CnC dispersion was then immersed in CCl_4 containing pS-nh_2 ligands, after a two-minute waiting period. Due to the density difference between CCl_4 and water, the shaped

aqueous phase rises out of the mould. as the shaped liquid rises, the sys- tem begins to reduce the interfacial area, the CnC surfactants jam, and the shape is fixed. as will be seen later, the shape of the liquid object can be changed subsequently by applying an external force, such as an electric field, shear, or change in the ph.

a technique used by liu *et al.* in their work on aqueous tubules was used to estimate the areal density of the CnCS at the oil–water interface as a function of time and aqueous ph (Figure 9.9). For all-liquid moulding, high rates of CnCS formation, assembly, and jamming are necessary to lock in the shape of the mould. Just as in the work by liu *et al.*, reducing the ph of the system led to more rapid assembly and higher density of CnCS, which correlated with a lower interfacial tension as measured using pendant drop tensiometry (Figure 9.9a). The observations of particle den- sity and the fidelity of the moulded liquid shape correlate well with one another; more rapid assembly of the CnCS led to improved reproduction of the mould (Figure 9.9b). The mechanism of shape stabilization is syn- ergistic: the CnCs adsorb to the liquid–liquid interface, and the ligands render them irreversibly bound to it. in the absence of the CnCs in the aqueous phase, the functionalized polymer acts as a surfactant, but can- not support the anisotropic surface stresses required to sustain the non-equilibrium shapes. in contrast to the water–toluene interface studied by liu *et al.*, CnCs spontaneously adsorbed to the water–CCl_4 interface. as such, in the presence of CnCs in the aqueous phase, the CnCs segregate to the interface (and interfacial tension decreases), but when the liquid rises from the mould, the resulting structure also collapses to a spherical shape (Figure 9.9b). only in the presence of both the ligands and the CnCs does the adsorption energy of the particles become sufficiently high, such that moulded liquids can be produced.

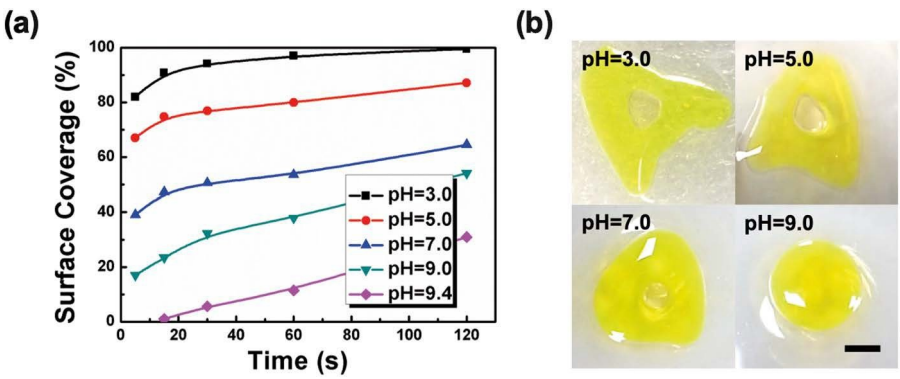

Figure 9.9 Surface coverage of CnCSs at the interface and moulded liquids in different ph. (a) CnCS density as a function of time and aqueous ph.
(b) Dyed liquid letter ‘a’ moulded in different ph. [CnC] = 10

mg ml^{-1}, [pS-nh_2] = 10 mg ml^{-1}, [na-fluorescein] = 0.1 mg ml^{-1}. Scale bar = 5 mm. reproduced from ref. 66 with permission from John Wiley and Sons, © 2018 WileY-VCh Verlag gmbh & Co. Kgaa, Weinheim.

as well as forming interfacially jammed systems, CnCs can act as bulk rheology modifiers for the aqueous phase. if the ph of the CnC disper- sion is decreased to 1.2, the CnCs aggregate, forming a weak, hydrogel network within the aqueous phase. if a dispersion of the CnCs at a ph of
1.2 is poured into the mould and, two minutes later, the filled mould is placed in a CCl_4 solution of pS-nh_2, a shaped CnCS-coated gel rises from the mould with high-fidelity transfer of the shape of the mould. here, the sharpness of the apex of the 'a' and the squareness of the edges and side- walls of the letter are replicated with excellent fidelity. in addition, the gel imparts extra mechanical strength to the shaped letter. Somewhat surpris- ingly, if the polymer ligands are not present, the gel solution alone cannot maintain the shape once immersed in CCl_4 and, when the gel rises out of the mould, the gel deforms into an irregular triangular-shaped drop- let. This coupling of bulk and interfacial mechanical properties results in structures that are far more robust than either the interfacially or the bulk- structured shapes. This result is somewhat surprising, given the rather small mechanical moduli we expect the interfacial film to possess due to its negligible thickness (≤100 nm), and is the subject of active investigation by our group.

9.6 Reconfigurability in Printed and Moulded Liquids

one of the most interesting properties of both structured liquid materials and the npS used to structure them is that they are inherently reconfigu- rable. This property was first demonstrated by huang *et al.*, who studied pendant drops that were structured into complex shapes by silica and polystyrene (pS) npS.[25] among a number of other experiments, huang *et al.* dispersed 5 mg ml^{-1} Cooh-functionalized pS nps in an aqueous phase that also contained diphenyliodonium chloride (DpiC, a photo- acid generator). The external oil phase was silicone oil in which 10% w/w pDmS-nh_2 had also been dispersed. Working at a ph range where the
-Coo^- groups were deprotonated and the –nh_3^+ groups were protonated (approximately ph 5–7) resulted in the formation of jammed npS layers at the oil–water interface (Figure 9.10). Spherical droplets on which npS had formed could then be deformed by an electric field and locked in shape, much like in the work of Cui *et al.*[67] illuminating the droplets with uV radiation drives a rearrangement of the aromatic groups in the DpiC and the production of an acid, reducing the ph of the aqueous phase. This reduction in ph causes disassembly of the npS. Droplets that were locked in shape by jammed npS were then found to relax to equilibrium drop shapes when illuminated with uV light. Subsequent increase in the ph was then shown to result in droplets that could once more be locked into non-equilibrium

drop shapes by npS assemblies, demonstrating the generation of a cyclically reconfigurable, interfacially structured, liquid material.

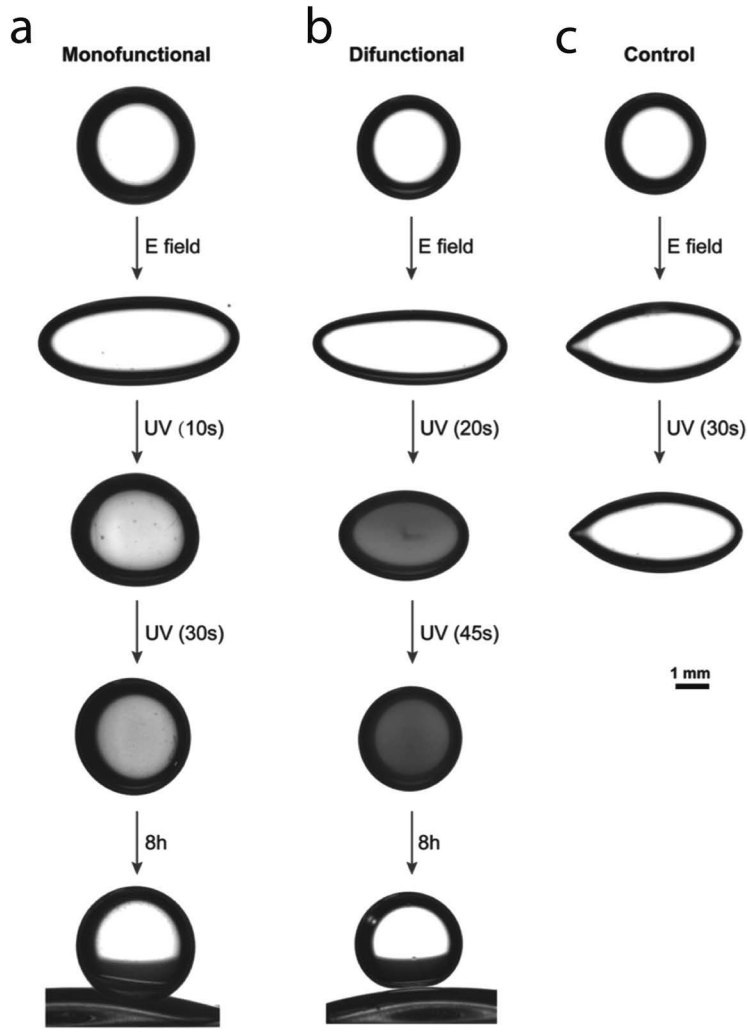

Figure 9.10 ph-reconfigurable, interfacially jammed, structured liquids. a water droplet containing Cooh-functionalized nanoparticles and a photo- acid generator is immersed in a bath of silicone oil containing nh_2- functionalized pDmS; and npS assemble at the oil–water interface. Deformation of the droplet using an electric field results in the formation of more npS; switching off the e-field results in the contrac- tion of the oil–water interface and the jamming of the npS monolayer, structuring the droplets into non-equilibrium shapes. uV illumina- tion of the sample reduces the ph of the aqueous phase, causing the disassembly of the npS and the relaxation of the droplet to a spherical shape. identical effects were observed with both (a) h_2n-pDmS-nh_2 and (b) pDmS-nh_2. (c) a control experiment with no DpiC present in the aqueous phase. reproduced from ref. 25 with permission from John Wiley and Sons, © 2016 WileY-VCh Verlag gmbh & Co. Kgaa, Weinheim.

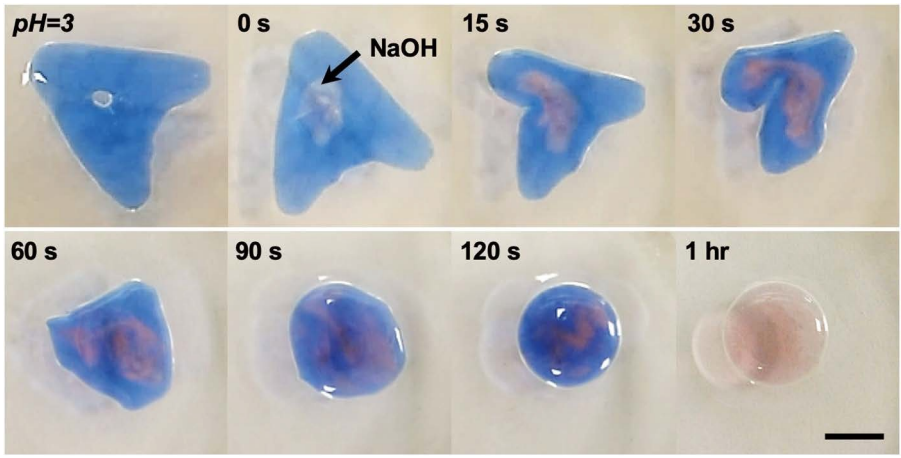

Figure 9.11 reconfigurable moulded liquids. Shape variation of dyed liquid letter 'a' with time in CCl_4 after adding ~10 µl naoh solution (0.1m) to the surface. [CnC] = 10 mg ml^{-1}, [pS-nh_2] = 10 mg ml^{-1}, [nile blue] = 0.05 mg ml^{-1}. Scale bar = 5 mm. reproduced from ref. 66 with permission from John Wiley and Sons, © 2018 WileY-VCh Verlag gmbh & Co. Kgaa, Weinheim.

Shi *et al.* exploited this ph-responsive, interfacial reconfigurability in their work on moulded liquids.[66] The ph response of the moulded liquids was probed by introducing ~10 µl of naoh solution (0.1m) to the triangular central hole of a moulded letter 'a' (Figure 9.11). nile blue was added to the aqueous CnC dispersion to monitor the change in the ph, where, for ph ≲ 10 the dye is blue and for ph ≳ 11 the dye changes to a red colour. The 'a' begins to deform almost immediately. The change in ph results in sub- stantially decreased binding strength of the CnCS, resulting in disassembly of the CnCS into ligands and CnCs, which diffuse back into CCl_4 and water, respectively. The colour change of the dye indicates transport of the naoh into the aqueous 'a'. one hour after naoh injection, the dye had diffused through the entire structure, and the 'a' collapsed to an equilibrium, spheri- cal shape, minimizing the interfacial area.

Similar effects of an identical origin were observed in the printed liquids of Forth *et al.* (Figure 9.12).[64] The different length scales and geometry of the printed liquids, however, give rise to some different phenomenology not seen in moulded liquids. The confining, fibrillar nature of the printed liq- uids means that disruption of the npS network at the interface causes local pressure differences and, hence, flow within the structures. heterogeneities in channel width at junctions and end-points of the printed liquids mean that flows terminate in these areas, leading to confinement of flows and the ability to locally reconfigure the printed structures.

This concept was demonstrated using solutions of naoh, and na- fluorescein (1 mg ml^{-1}) or nile blue dyes (1 mg ml^{-1}).

using a weakly

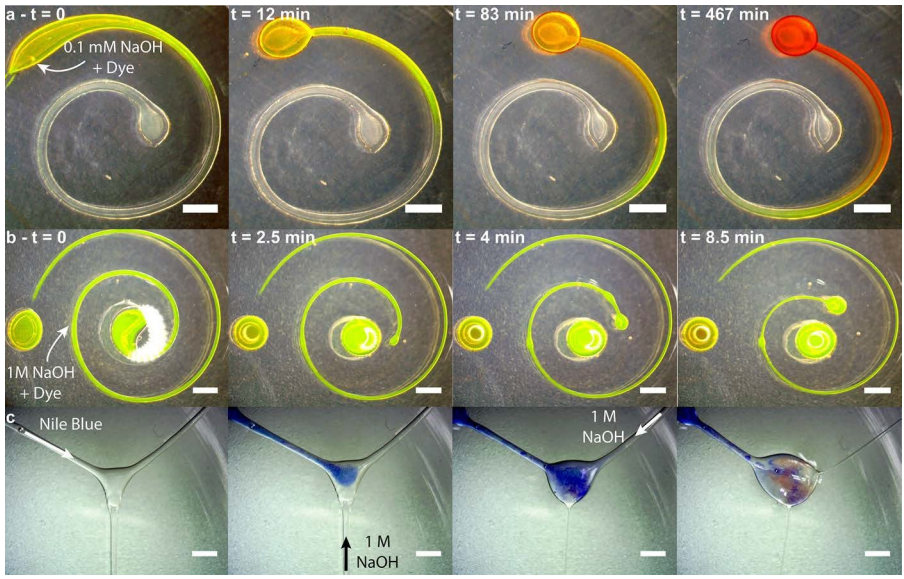

Figure 9.12 reconfigurable printed liquids. (a) The end terminal of an npS- stabilized, printed aqueous spiral is injected with na-fluorescein and naoh (0.1 mm). The aqueous phase is buffered with 5 mm nameS.
(b) injection of 1 m naoh and na-fluorescein into a similar spiral results in break-up of the npS network and relaxation of the printed spiral on the timescale of ~10 minutes. (c) Sequential injection of nile blue and 1 m naoh into the different terminals of a branched structure (the change in colour of the dye to red is indicative of a basic ph). all scale bars, 2 mm. reproduced from ref. 64 with per- mission from John Wiley and Sons, © 2018 WileY-VCh Verlag gmbh & Co. Kgaa, Weinheim.

buffered aqueous phase (5 mm meS) limits the spatial extent of ph change on short timescales. injecting an aqueous spiral (diameter, 200 µm) with naoh (0.1 m) and na-fluorescein results in a ph change that is insufficient to break up the npS network, and the spiral remains intact (Figure 9.12a). Dye then slowly diffuses through the intact structure. by contrast, inject- ing more concentrated naoh (1 m) causes disassembly of the npS at the oil–water interface and relaxation of the printed liquid. The extent of relax- ation depends on the concentrations of naoh used, meaning that partial desorption of the npS and narrowing (rather than relaxation to a spheri- cal geometry) of the channels can be achieved (Figure 9.12b). Finally, local reconfiguration of the branched structure was studied (Figure 9.12c). injec- tion of 1 m naoh and nile blue into each of the termini of the branched structure resulted in local relaxation of the printed structure, leaving the remainder unaltered. narrowing of the channels drives internal flows and alteration of local ph (note the change in colour of the nile blue at the intersection of the channels).

it is important to note that npS can also be made responsive to a num- ber of other stimuli. recently, Zhang *et al.* used a zwitterionic surfactant to disrupt the binding between ligand-stripped ('naked') magnetic Fe_3o_4 nanocrystals and pDmS-nh_2.[39] Similar results to those of huang *et al.* were obtained while using far more exotic, application-relevant materials. Furthermore, Zhang *et al.* were able to show that solid-like assemblies of mag- netic nanocrystals exhibited a strong response to an external magnetic field, suggesting potential in the generation of liquid actuators. addition of the zwitterionic surfactant caused the relaxation of jammed, solid-like interfaces and the adoption of equilibrium shapes by the nanocrystal surfactant-coated droplets, with a corresponding reduction in the magnetic response of the system. most recently, and perhaps most remarkably, liu *et al.* have shown that Fe_3o_4 nanoparticles form assemblies of npS in the presence of polyhe- dral oligomeric silsesquioxane, which, when jammed, form ferromagnetic monolayers, leading to the production of reconfigurable, ferromagnetic liq- uid droplets.[68]

9.7 All-liquid Microfluidics: Combining Liquid 3D Printing, Patterned Substrates, and Heterogeneous Catalysis at the Oil–Water Interface

The work discussed so far has used the arrest of hydrodynamic instabili- ties through interfacial jamming to produce free-floating objects of water in oil. This property makes the structures inherently autonomous, *i.e.*, they can be moved (or perhaps even made to move themselves) and eas- ily reconfigured spatially in response to an external stimulus. however, not being bound to a substrate makes them challenging to produce and makes it extremely difficult to generate two identical structures. Furthermore, the systems are difficult to manipulate, limiting their use in micro- fluidics applications, which is one of the most promising immediate uses of these materials.

To overcome this limitation, Feng *et al.* harnessed photopatterned sub- strates to confine an aqueous phase to a predetermined geometry.[69] by generating patterns of hydrophilic and superhydrophobic regions, surface wetting and contact line pinning could be harnessed to reproducibly make highly controlled semi-cylindrical tubules of water. Dispersing highly charged nanoclays in the aqueous phase, and polymer surfactants of a complemen- tary functionality in an oil phase in which the substrate was immersed, led to the assembly of nanoclay surfactants at the oil–water interface. These nanoclay surfactants in turn formed a semi-permeable membrane, which could be exploited to harness the structured liquid paradigm to fabricate a new class of 3D all-liquid microfluidic devices with bespoke

properties. in this section, we show how these concepts can be applied to produce flow

channels that are architected with controlled dimensionality using micro- patterned 2D substrates and liquid-in-liquid 3D printing, and a broad palette of immiscible liquids. Their potential for rendering chemical systems of arbi- trary complexity to perform tasks, including chemical separations, catalyst immobilization, multistep chemical transformations, and chemical logic, is also highlighted.

glass supports are first coated with a porous superhydrophobic polymer that was photopatterned with a variety of superhydrophilic channel architec- tures (Figure 9.13). The polar phase, *e.g.*, an aqueous dispersion of anionic 2D nanoclays (10 mg ml^{-1} at ph 7.0), is then deposited onto the superhydro- philic region prior to immersion in an oil phase, *e.g.*, a solution of homotel- echelic amine-terminated poly(dimethylsiloxane) (h_2n-pDmS-nh_2, M_n ~27 kg mol^{-1}, 10% w/w) in either toluene, silicone oil, or dodecane (Figure 9.13a). once the liquid phases are in place on the patterned glass support, npS film formation at the water–oil interface is spontaneous. The system reaches its

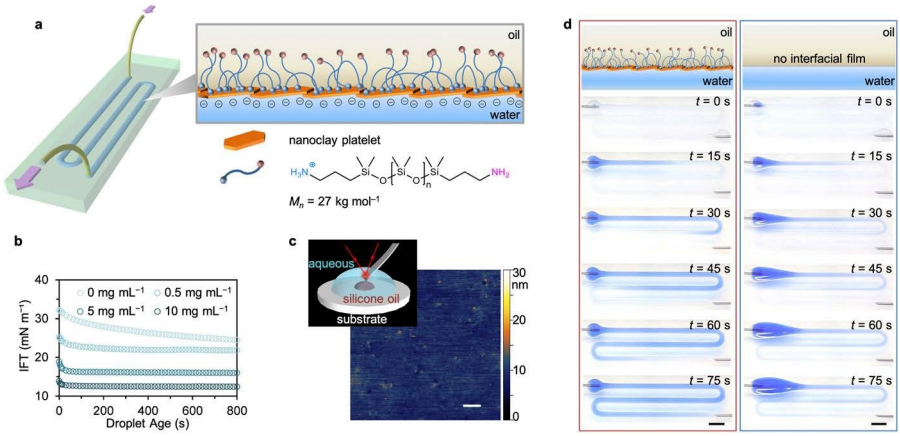

Figure 9.13 all-liquid microfluidic devices stabilized by self-forming nanoclay– polymer surfactant walls at the liquid–liquid interface. (a) Schematic of an all-liquid microfluidic device comprised of immiscible liquid phases confined in space using superhydrophobic–superhydrophilic micropatterned substrates. nanoclay–polymer surfactants (npSs) self-assemble at the liquid–liquid interface, forming an elastic wall that allows the all-liquid architecture to maintain integrity while fluid is pumped through the channel. (b) Temporal evolution of inter- facial tension (iFT) of aqueous nanoclay dispersions (0.5, 5, and 10 mg ml^{-1}, ph 7.0) introduced to solutions of h_2n-pDmS-nh_2 in tolu- ene (10% w/w), illustrating control over the rate of npS assembly at the interface. (c) *In situ* aFm image of the npS film. The inset shows the schematic diagram of the experimental setup for aFm measure- ments. Scale bar, 100 nm. (d) Time-lapse images of a solution of blue dye being pumped (10 ml h^{-1}) through the channel in the presence (left) and in the absence (right) of the npS film. Scale bars, 5 mm. reproduced from ref. 69, https://doi.org/10.1038/s41467-019-09042-y, under the terms of the CC bY 4.0 license,

steady state rapidly, typically within 30 seconds (Figure 9.13b). The topogra- phy of these well-packed nanoclays at the liquid–liquid interface was revealed using *in situ* atomic force microscopy (aFm, Figure 9.13c).

interfacial forces between the liquids and solid substrate are effective in pinning and confining the aqueous phase in arbitrarily complex geome- tries and a wide range of channel widths (635–3000 μm). importantly, these nanoclay–nanoclay interactions ultimately determine the unique mechanical properties of the npS films for both compressive and extensive stresses, ren- dering patterned all-liquid microchannels that are shape-persistent under high flow rates, even at sharp curves defined by superhydrophilic surface patterns: *e.g.*, in u-bends of serpentine channels. only patterned microchan- nels bearing npS walls were capable of guiding flow along the channels at these rates without aberrations to the all-liquid architectures. in the absence of these elastic npS walls, the aqueous phase accumulates at the entry point of the channel without flowing along the path determined by the patterned substrate (Figure 9.13d).

The nanoclays we use here yield npS assemblies that are selectively per-
meable to solutes in either liquid phase. We demonstrated selective mass transfer across the interface (Figure 9.14a) by carrying out cross-over

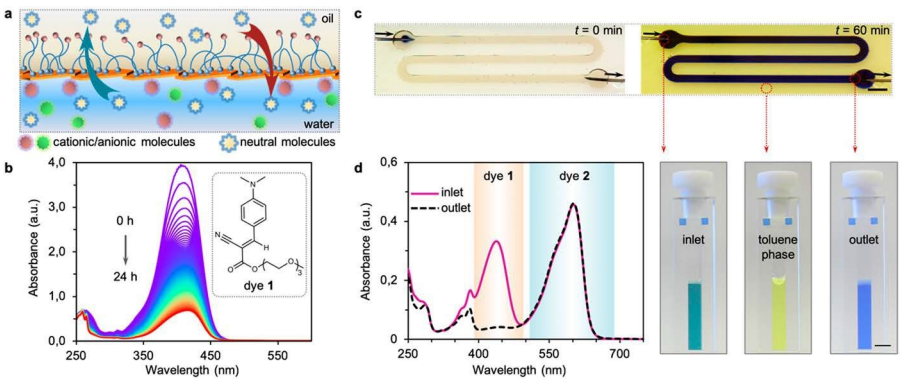

Figure 9.14 probing the semi-permeability of 2D nanoclay–surfactant films assembled at a liquid–liquid interface. (a) Schematic showing selec- tive mass transfer across the water–oil interface through the npS film.
(b) Stacked uV–vis spectra of a neutral dye (**1**) at 5 min time inter- vals, monitoring dye transfer from water to toluene across the npS membrane film in a masked cuvette. The inset shows the chemical structure of dye **1** engaged in mass transfer. (c) a microfluidic device depicting the flow of a mixed solution of dye **1** and resazurin sodium
(**2**) for chemical separation. [**1**] = 1.4 mg ml^{-1}, [**2**] = 1 mg ml^{-1}. pho- tographs of the diluted inlet, outlet, and overlay of toluene solutions collected in cuvettes show the dye separation after infusing the mixed solution at a flow rate of 0.2 ml h^{-1} for 1 h. Scale bar, 5 mm. (d) uV–vis spectra of the diluted inlet and outlet solutions used to quantify the

efficiency of dye **1** partitioning from the aqueous phase to the toluene phase. reproduced from ref. 69, https://doi.org/10.1038/s41467-019- 09042-y, under the terms of the CC bY 4.0 license, http://creativecommons.org/licenses/by/4.0/. Copyright 2019, The authors.

experiments using a charge-neutral fluorescent dye (dye **1**, Figure 9.14b) that has an affinity for both water and toluene, and compared the cross-over rate with those of anionic resazurin (dye **2**) and cationic rhodamine 6g (dye **3**). in a quartz cuvette, an npS interfacial film was formed after introducing sil- icone oil containing h_2n-pDmS-nh_2 surfactant on top of an aqueous phase, a dispersion of nanoclays (9 mg ml^{-1}), and dye (100 µg ml^{-1}). Toluene was added into the oil phase afterwards. by monitoring the optical absorbance of the aqueous phase, only the partitioning of charge-neutral dye **1** into the toluene was observed (Figure 9.14b). The partitioning of charge-neutral dye **1** in the micropatterned all-liquid device was further confirmed using laser scanning confocal microscopy (lSCm), suggesting that the semi-permeable npS film could be utilized for inline chemical separation under flow. a solution of dyes **1** and **2** was pumped through the channel (0.2 ml h^{-1}) to demonstrate this feature. after ~1 h under continuous flow, more than 93% of dye **1** was separated from the aqueous dye mixture by liquid–liquid par- titioning into the toluene phase; dye **2** was retained in the microchannel (Figure 9.14c and d).

beyond their use as structuring elements, anionic nanoclays further

allow cationic molecules, enzymes, and nanoparticles to be anchored to the npS wall (Figure 9.15a–c). Cationic small molecules were immobilized

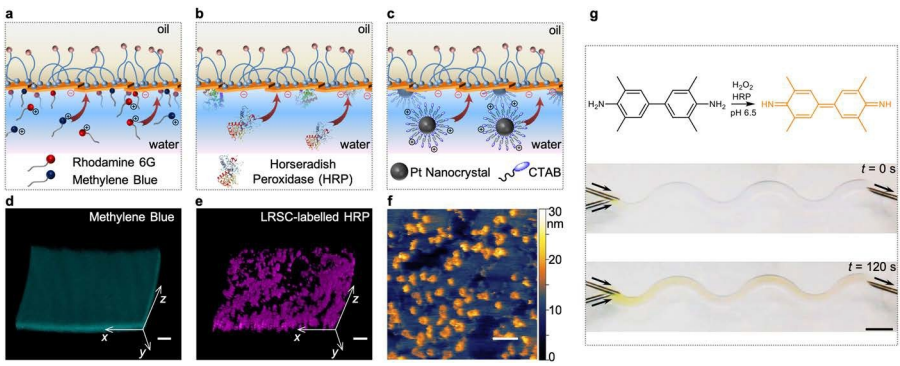

Figure 9.15 anionic nanoclay–polymer surfactant films assembled at the liq- uid–liquid interface serve as a support for cationic catalysts. (a–c) Schematic of the anchoring of cationic molecules (a), enzymes (b), and nanocrystals (c) to the anionic npS film lining the microchan- nels. (d, e) 3D reconstitution of confocal images of methylene blue (d) and lrSC-labelled hrp (e) to determine the adhesion of cationic species to the npS wall of the microchannel. Scale bars, 100 µm. (f) *In situ* aFm image of the npS film immobilized with CTab-coated pt nanocrystals at the water–silicone oil interface. Scale bar, 100 nm. (g) oxidation of Tmb substrate catalysed by immobilized hrp in the microchannels, which generates products with distinctive colours under flow. Scale bars, 5 mm. reproduced

from ref. 69, https://doi. org/10.1038/s41467-019-09042-y, under the terms of the CC bY 4.0 license, http://creativecommons.org/licenses/by/4.0/. Copyright 2019, The authors.

on the nps walls by using iscm to visualize the spatial distribution of methylene blue (Figure 9.15d) and rhodamine 6g in the device. after pumping cationic dyes into the microchannel, aging the system such that they diffuse to the interface, and rinsing with water to remove unbound objects, the immobilized fluorophores each tracked the curvature of the nps wall. Similarly, cationic enzymes (*e.g.*, horseradish peroxidase, hrp) as well as cationic nanocrystal catalysts (*e.g.*, cetyltrimethylammonium bromide (CTab)-modified pt nanocrystals, $\zeta = +19.2 \pm 1.3$ mV) are able to anchor to the wall as well. While the fluorescence of adsorbed dye- labeled hrp (irsc-labelled hrp) was readily visualized using iscm (Figure 9.15e), the immobilization of CTab-pt nanocrystals with respect to the underlying nanoclay tiles at the liquid–liquid interface required *in situ* afm to properly visualize nanocrystal density (Figure 9.15f). With these catalysts in place, all-liquid microfluidic devices are primed for biphasic chemical synthesis. Flow-driven multistep chemical transformations were carried out using all-liquid microfluidic devices config- ured with hrp at nps walls. a solution of 3,3′,5,5′-tetramethylbenzidine (Tmb) and hydrogen peroxide (Figure 9.15g), or a solution of phenol, 4-aminoantipyrine, and hydrogen peroxide, was pumped through the channel (1 ml h^{-1}), which led to oxidation of the colourless substrates to coloured products.

9.8 Bijels by Direct Mixing

The methods discussed so far have used interfacial jamming to arrest hydro- dynamic instabilities in liquids that are pre-formed into highly controlled geometries. These techniques produce small volumes of well-defined sys- tems that can be readily manipulated and exploited for a range of potential applications. however, channel sizes in these materials are typically large, the lower limit produced so far being 10 μm. Furthermore, the volume of material that can be produced with these methods is limited, with production time per unit volume of material increasing rapidly as channel width decreases. a highly desirable goal is to produce a material with a similar mor- phology to the tortuous bijels produced *via* spinodal decomposition using a method that is less challenging to work with. remarkably, bijel-like morphol- ogies can be generated simply by shaking or stirring immiscible liquids in the presence of nanoparticle surfactants.

This observation was recently made by two different groups, working inde- pendently of one another.[70,71] huang *et al.* studied a system comprising an aqueous phase containing cooh-functionalized nps and a non-aqueous phase containing nh_2-functionalized polymer surfactants. Taking approxi- mately equal volumes of the aqueous and non-aqueous phases, using a single molecular weight of polymer surfactant, and shaking the system on a vortex mixer was found to give rise to emulsions of one liquid inside of the other. remarkably, when a mixture of

molecular weights of polymer surfactant was used, bijel-like structures consisting of extended domains of both liquids were observed (Figure 9.16).

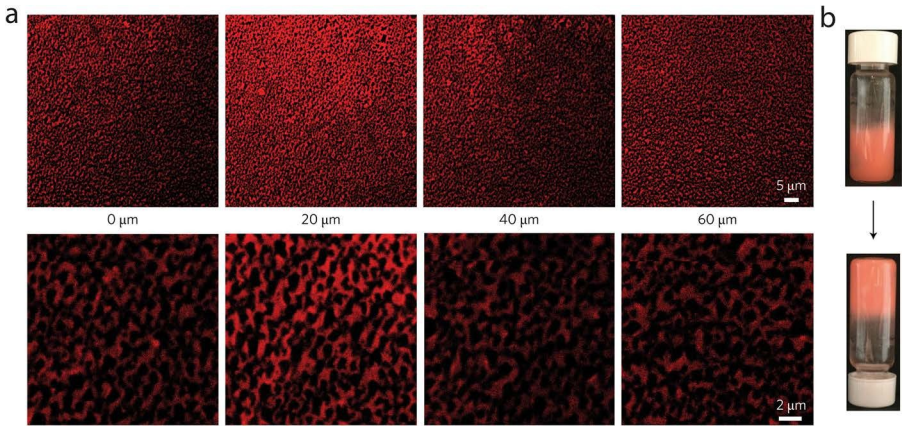

Figure 9.16 Small-domain bijels obtained by vortex mixing. (a) high- and low- magnification confocal micrographs of a 'bijel' made by vortex mix- ing equal volumes of an aqueous dispersion of pS nanoparticles (10 mg ml^{-1}) and pDmS-nh_2. Distances correspond to the distance the objective was moved vertically from the base of the sample. note that high-magnification images were obtained by oversampling. (b) Vials containing bijels made by vortex mixing are inverted and photo- graphed before and after one week. The non-aqueous phase (toluene) is dyed with nile red. reproduced from ref. 70 with permission from Springer nature, Copyright 2017.

optical sections were taken of the bijels as far as 60 μm into the sample (beyond which optical extinction prevents imaging), showing the presence of the extended liquid domains. What is most striking about the result is the size of the domains (Figure 9.16a). Confocal micrographs showed that chan- nel widths as small as 1 μm could be achieved simply by using high-enough concentrations of particles (10 mg ml^{-1} 16.5 nm polystyrene particles). The domain size, r_d, exhibited the expected approximate scaling with particle concentration, c, (*i.e.*, $r_d \sim c^{-1}$), while it was also shown that both the particles and the polymer surfactants must be present in order for the 'bijels' to form. The effect was also shown to be generalisable to several different solvents (both decane and toluene) and different types of polymer surfactants (both amine-functionalized polystyrene and amine-functionalized pDmS). invert- ing vials in which the bijels had been produced did cause the bijels to flow over the course of a week, demonstrating the presence of a yield stress in the system (Figure 9.16b).

The result of huang *et al.* is phenomenologically remarkable, but it is not clear why simply shaking two immiscible liquids should give rise to such a structure. The work of Cai *et al.*, and follow-up work by li *et al.* and macmillan *et al.*, which combined systematic investigation of the formation of bijels by stirring in tandem with careful formulation optimisation, pro- vides some insight here (Figure 9.17).[71–73] This work studied a variant of the

nanoparticle surfactant system developed by ravera *et al.*,[74,75] in which

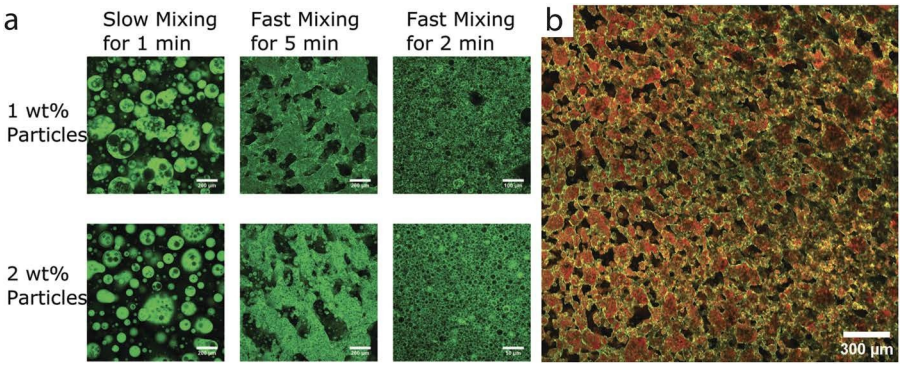

Figure 9.17 bijels formed by stirring. (a) Confocal micrographs of systems com- prising silica nanoparticles and CTab in glycerol and silicone oil after being subjected to different, sequential mixing procedures. (b) Con- focal micrograph of the bijel made using the optimised mixing pro- cedure. The red regions are nile red-dyed glycerol and the green is FiTC-labeled silica nanoparticles. reproduced from ref. 71 with per- mission from the royal Society of Chemistry.

silica nps and cetyltrimethylammonium bromide (CTab, a cationic surfac- tant) are dispersed in a polar phase. The CTab modifies the surface chem- istry of the nanoparticles *in situ*, forming CTab-SinpS that readily adsorb to the liquid–fluid interface. Cai *et al.* prepared their nanoparticles in glycerol and then added a second phase of immiscible silicone oil, which consisted of a mixture of equal weights high- and low-viscosity silicone oil (10 000 cSt and 50 cSt). The stirring protocol, which involved an initial slow mixing at 200 rpm for 1 minute followed by a more rapid mixing for 5 minutes, was found to be critical to the generation of CTab-SinpS-stabilized liquid bicon- tinuous structures.

both results are fascinating and significant, since they show that extended, liquid bicontinuous domains can be produced *without* using spinodal decomposition.[76] unsurprisingly, however, there appear to be a number of differences between the systems produced by direct mixing and the more elegant systems produced by spinodal decomposition. First, bijels produced by direct mixing lack a single well-defined length scale. While an approximate domain width can be estimated, Fourier trans- forms of confocal micrographs of these systems lack the characteristics of the presence of a dominant length scale, as seen in systems produced by spinodal decomposition.[1] Second, the extent of bicontinuity in these systems is unclear. one of the major features of bijels formed by spinodal decomposition is the presence of two interpenetrating domains that per- colate the entire span of a sample (Chapter 1). This opens up a whole wealth of potential applications in chemical synthesis (*i.e.*, as a membrane contactor) or in energy storage.[21,77,78] it is not apparent from the images in either paper that a percolating pathway exists in bijels produced by either

of the direct methods. That said, these systems have a number of advan- tages that open up applications in several different fields. many of these sectors are inaccessible to traditional bijels, as production *via* spinodal decomposition has proven difficult to scale beyond millilitre-level production, while batch shaking and stirring is, in principle, significantly more scalable. The presence of a yield stress suggests interesting applications in formulating soft materials in which sedimentation on long timescales causes spoilage, such as in personal care, skin care, and agrochemicals. The quasi-bicontinuous structure of these systems could prove useful in the encapsulation of compounds in edible products, as well as in the formulation of fragrances and personal care products. Finally, while the methodical work of Cai, li, and macmillan *et al.* provides some insight into how stirring might give rise to liquid bicontinuous structures, the actual mechanism by which these structures are formed, and how they might be controlled, is still very much unknown.

9.9 Perspective and Future Prospects

Significant progress has been made in understanding the formation, assembly, and jamming of npS at fluid–fluid interfaces and in using this interfacial jamming to produce structured, all-liquid materials. Yet, while many questions have been answered, at least as many new questions have emerged. The fluid–fluid interface provides a unique platform to address some very fundamental, long-standing questions in materials science. up to this point the nanoparticles themselves have been treated as objects without inherent function beyond simple reconfigurability, yet that is far from being the case.

From a fundamental perspective, manipulating the non-equilibrium states of interfacial assemblies of nanoparticles provides a truly unique opportunity to shed light on the complex physics of systems that cannot relax to equilibrium. glassy or jammed systems are not actively driven but instead are subject to an intrinsic irreversibility arising from extremely long correlation times.[79,80] efforts to understand the origins of such extraordi- narily slow relaxations have revealed many peculiarities of vitrified liquids, including dynamic heterogeneities, extreme sensitivity to boundary con- ditions, non-monotonic history dependence, non-classical transport laws, fictive temperatures, and large multipoint susceptibilities.[81,82] remarkably, these anomalous properties are seen over a very small range of macroscopic control parameters and are accompanied by almost negligible changes in microscopic structure.

by tailoring the size, shape, and functionality of the nps, while con- trolling their interactions and response to various external forces, one can navigate around and through the phase space of glassy behavior. The recent advances in transmission electron microscopy on liquids will enable map- ping of the spatial location

of each np surfactant at the fluid–fluid interface in real space and in real time, allowing their movement to be tracked over

a broad range of timescales, and characterize the heterogeneous nature of the assemblies.[83–86] Detailed tracking of particles comprising supercooled liquids and glasses has been achieved previously with confocal microscopy of dense colloidal dispersions.[87] however, the fundamental timescale of particle motion in those systems has generally limited experimental studies to dynamical regimes that can be much more readily probed with com- puter simulations. The npS systems feature relaxation times that are several orders of magnitude shorter. Jammed interfacial np assemblies present an opportunity to extend detailed observations that are significantly beyond the reach of simulations, potentially providing access to the emergent length scales predicted by competing theories for glass transition. With the low frequency, real-space npS tracking afforded by transmission elec- tron microscopy, in concert with X-ray photocorrelation spectroscopy and fluorescence recovery after photobleaching, unprecedented detail into the static and dynamic behaviour of 2D systems that can form a glass or jam can be obtained, providing fresh insight into the basic physical nature of the glass transition and benchmarking relevant timescales for the structur- ing of liquids.

in this chapter, we have focused on high surface tension systems that tend to be mechanically robust and respond to large changes in their envi- ronment (ph, chemical composition, or mechanical stress). an extremely low surface tension system should not only be affected more strongly by thermal fluctuations, but also yield systems that can be reconfigured easily and that respond to small changes in their external environment. one low surface tension system is water-in-water emulsions (Chapter 5): aqueous dispersions of partially miscible polymers that phase separate, forming domains with surface tensions of the order of 1 µn m^{-1}.[88,89] Stable water- in-water emulsions can be formed using micro- and nanoparticles, such as cellulose nanocrystals, aluminium hydroxide nanoplates, and silica par- ticles, or by the complexation of oppositely charged polyelectrolytes.[90–92] both nanoparticle–polyelectrolyte and polyelectrolyte–polyelectrolyte complexation can be used to generate capsules with markedly different mechanical properties and compartmentalized, cell-like bodies can be produced.[93–96] Studies in several different laboratories are pursuing all- aqueous systems to generate a wide range of structures with continuous geometries by 3D printing, allowing easy diffusion of reactants across the water–water membrane.[97]

a well-studied aqueous two-phase system that is amenable to 3D printing applications is that of aqueous solutions of dextran and polyethyelene oxide. With polyanions (pa) dissolved in one solution and polycations (pC) in the second, the diffusion and interactions of the pa and pC to the interface results in the formation of a coacervate that can support anisotropic surface stresses and shape the water–water system into complex shapes. This compartmen- talizes one aqueous phase in a second, separating the two by an asymmetric pa/pC coacervate

membrane, where the diffusion of charged species across the interface is highly directional. anions flow in one direction only and

cations in the other. using redox materials with opposite charges the possi- bility exists to produce an aqueous flow battery. For example, methyl violo- gen with a positive charge can be dissolved in polyethylene glycol solutions with polyanions, and potassium ferrocyanide can be mixed with dextran and polycations. Coupled to two electrodes to construct an electric circuit, the redox materials could, in principle, be confined in the two aqueous phases in both the charged and discharged states and be stored into containers after collecting with pumps. by controlling the concentration of redox materials and polyelectrolytes, and regulating the flow rate of the pump, the perfor- mance of the aqueous flow battery can be tuned. This platform represents an entirely new class of material that has distinct advantages. The redox mate- rials can easily be changed to vary the potentials. Conventional membranes for separation are removed, decreasing the cost of the battery. This aqueous flow battery can be printed using a 3D printer, allowing the battery design and structure to be tailored.

up to this point the functional properties nanoparticles themselves

have been hugely underexploited. gold nps exhibit plasmonic proper- ties that can impart mirror-like optical properties to an interface when the nps or npS are densely packed.[28] nps can also be conductive, so that, when the nps or npS jam at the interface and a percolating path- way is formed, the assembly becomes conductive in the plane of the films. Studies on mXenes and 2D chalcogenide crystals show a similar behaviour for the interfacial assemblies.[98] While the conductivity can be used as an indicator of jamming, the more exciting potential lies in the fact that the interface surrounding a droplet or a tubule is conduc- tive. Coupling this to the multitude of geometries that can be 3D printed affords direct access to generating 3D all-liquid devices, like solenoids or even transistors.

all of the systems considered thus far either approach equilibrium or are prevented from doing so by jamming. Why not deliberately drive the system out of equilibrium by encapsulating active swimmers that con- vert chemical energy into kinetic energy in a tunable manner through the use of active filament or nanoparticle systems? These systems consist of rigid or semi-rigid micrometre-length rod-shaped protein assemblies dispersed in water, or composite hard particles geometrically designed to propel the particles in the presence of an accelerant. actin or tubulin rods, for example, become active swimmers in the presence of a molecu- lar motor with the addition of aTp, along with a depletant to increase the interaction between the constituent components of these systems.[99–102] The molecular motors drive the motion of the rods, resulting in an active system of rods in which the strength of the activity can be tuned by the addition of aTp. When appropriately confined, the systems can be made to swim coherently.[101] From a theoretical perspective, such active systems have only been studied under periodic and solid boundary conditions and not under soft

confinement, as would be the case in an interfacially structured liquid system. These assemblies will be materials that evolve

non-gaussian surface fluctuations, the properties of which are distinct from conventional materials. The force of the filaments impinging on the soft confines will cause the walls to deform, causing the confining geom- etry to change or evolve with time. harnessing these effects would allow us to produce an entirely new type of biologically inspired material that drives itself from equilibrium.

Finally, an elephant in the room must be confronted; one of the major shortcomings of this field is an impactful real-world application that has been successfully translated from the laboratory into industry. bluntly, bijels currently lack a 'killer app'. There has been some success in attracting invest- ment into high-value, emulsion-based printed materials, although this argu- ably falls more into the class of more traditional emulsion science (albeit in an extremely advanced form).[103–105] That said, the field is still in its infancy, with bijels only having been first produced in 2007.1 it may be that signif- icant progress in translating bijels out of the laboratory and into a useful product is just around the corner.

Acknowledgements

This work was supported by the u.S. Department of energy, office of Science, office of basic energy Sciences, materials Sciences and engineering Division under Contract no. De-aC02-05-Ch11231 within the adaptive interfacial assemblies Towards Structuring liquids program (KCTr16).

References

1. e. m. herzig, K. a. White, a. b. Schofield, W. C. K. poon and p. S. Clegg, *Nat. Mater.*, 2007, **6**, 966–971.
2. K. Stratford, r. adhikari, i. pagonabarraga, J.-C. Desplat and m. e. Cates, *Science*, 2005, **309**, 2198–2201.
3. m. reeves, K. Stratford and J. h. J. Thijssen, *Soft Matter*, 2016, **12**, 4082–4092.
4. m. reeves, a. T. brown, a. b. Schofield, m. e. Cates and J. h. J. Thijssen, *Phys. Rev. E*, 2015, **92**, 032208.
5. F. Jansen and J. harting, *Phys. Rev. E*, 2011, **83**, 046707.
6. D. Cai and p. S. Clegg, *Chem. Commun.*, 2015, **51**, 16984–16987.
7. g. Di Vitantonio, T. Wang, m. F. haase, K. J. Stebe and D. lee, *ACS Nano*, 2019, **13**, 26–31.
8. m. F. haase, h. Jeon, n. hough, J. h. Kim, K. J. Stebe and D. lee, *Nat. Commun.*, 2017, **8**, 1234.
9. m. F. haase, n. Sharifi-mood, D. lee and K. J. Stebe, *ACS Nano*, 2016, **10**, 6338–6344.
10. m. F. haase, K. J. Stebe and D. lee, *Adv. Mater.*, 2015, **27**,

7065–7071.
11. S. boakye-ansah, m. S. Schwenger and m. F. haase, *Soft Matter*, 2019, **15**, 3379–3388.

12. Y. montelongo, D. Sikdar, Y. ma, a. J. S. mcintosh, I. Velleman, a. r. Kucernak, J. b. edel and a. a. Kornyshev, *Nat. Mater.*, 2017, **16**, 1127–1135.
13. m. Zhang, I. Wei, h. Chen, Z. Du, b. p. binks and h. Yang, *J. Am. Chem. Soc.*, 2016, **138**, 10173–10183.
14. T. li, F. nudelman, J. W. Tavacoli, h. Vass, D. J. adams, a. lips and p. S. Clegg, *Adv. Mater. Interfaces*, 2016, **3**, 1500601.
15. T. li, g. brandani, D. marenduzzo and p. S. S. Clegg, *Phys. Rev. Lett.*, 2017, **119**, 018001.
16. J. Forth and p. S. Clegg, *Langmuir*, 2016, **32**, 6387–6397.
17. m. graužinytė, J. Forth, K. a. rumble and p. S. Clegg, *Angew. Chem., Int. Ed.*, 2015, **54**, 1456–1460.
18. J. Forth, D. J. French, a. V. gromov, S. King, S. Titmuss, K. m. lord, m. J. ridout, p. J. Wilde and p. S. Clegg, *Langmuir*, 2015, **31**, 9312–9324.
19. b. p. binks, *Langmuir*, 2017, **33**, 6947–6963.
20. b. p. binks and r. murakami, *Nat. Mater.*, 2006, **5**, 865–869.
21. m. e. Cates and p. S. Clegg, *Soft Matter*, 2008, **4**, 2132–2138.
22. p. S. Clegg, e. m. herzig, a. b. Schofield, S. u. egelhaaf, T. S. horozov, b. p. binks, m. e. Cates and W. C. K. poon, *Langmuir*, 2007, **23**, 5984–5994.
23. m. Cui, T. emrick and T. p. russell, *Science*, 2013, **342**, 460–464.
24. J. he, Z. niu, r. Tangirala, J. Y. Wang, X. Wei, g. Kaur, q. Wang, g. Jutz, a. böker, b. lee, S. V. pingali, p. Thiyagarajan, T. emrick and T. p. russell, *Langmuir*, 2009, **25**, 4979–4987.
25. C. huang, Z. Sun, m. Cui, F. liu, b. a. helms and T. p. russell, *Adv. Mater.*, 2016, **28**, 6612–6618.
26. a. Toor, b. a. helms and T. p. russell, *Nano Lett.*, 2017, **17**, 3119–3125.
27. V. a. Turek, m. p. Cecchini, J. paget, a. r. Kucernak, a. a. Kornyshev and J. b. edel, *ACS Nano*, 2012, **6**, 7789–7799.
28. p.-p. Fang, S. Chen, h. Deng, m. D. Scanlon, F. gumy, h. J. lee, D. momotenko, V. amstuts, F. Cortés-Salazar, C. m. pereira, Z. Yang, h. h. girault, D. Scanlon, p.-p. Fang, S. Chen, h. Deng, C. m. pereira and Z. Yang, *ACS Nano*, 2013, 9241–9248.
29. b. h. Kim, n. lee, h. Kim, K. an, Y. i. park, Y. Choi, K. Shin, Y. lee, S. g. Kwon, h. b. na, J.-g. park, T.-Y. ahn, Y.-W. Kim, W. K. moon, S. h. Choi and T. hyeon, *J. Am. Chem. Soc.*, 2011, **133**, 12624–12631.
30. Z. Yang, J. Wei, Y. i. Sobolev and b. a. grzybowski, *Nature*, 2018, **553**, 313–318.
31. m. grzelczak, J. Vermant, e. m. Furst and l. m. liz-marzán, *ACS Nano*, 2010, **4**, 3591–3605.
32. J. Vermant, *Nature*, 2011, **476**, 286–287.

33. r. a. peters, *Proc. R. Soc. B*, 1931, **109**, 88–90.
34. J. J. betts and b. a. pethica, *Trans. Faraday Soc.*, 1956, **52**, 1581.
35. C. huang, m. Cui, Z. Sun, F. liu, b. a. helms and T. p. russell, *Langmuir*, 2017, **33**, 7994–8001.
36. Y. lin, h. Skaff, T. emrick, a. D. Dinsmore and T. p. russell, *Science*, 2003, **299**, 226–299.

37. Z. Sun, T. Feng and T. p. russell, *Langmuir*, 2013, **29**, 13407–13413.
38. T. Feng, D. a. hoagland and T. p. russell, *Langmuir*, 2014, **30**, 1072–1079.
39. Z. Zhang, Y. Jiang, C. huang, Y. Chai, e. goldfine, F. liu, W. Feng, J. Forth, T. e. Williams, p. D. ashby, T. p. russell and b. a. helms, *Sci. Adv.*, 2018, **4**, eaap8045.
40. C. huang, Y. Y. Chai, Y. Jiang, J. Forth, p. D. ashby, m. m. l. arras, K. hong,
g. S. Smith, p. Yin and T. p. russell, *Nano Lett.*, 2018, **18**, 2525–2529.
41. a. marchand, J. h. Weijs, J. h. Snoeijer and b. andreotti, *Am. J. Phys.*, 2011, **79**, 999–1008.
42. l. gao and T. J. mcCarthy, *Langmuir*, 2009, **25**, 14105–14115.
43. l. gao and T. J. mcCarthy, *Langmuir*, 2006, **22**, 6234–6237.
44. J. Forth, p. Y. Kim, g. Xie, X. liu, b. a. helms and T. p. russell, *Adv. Mater.*, 2019, **31**, 1806370.
45. n. bizmark, m. a. ioannidis and D. e. henneke, *Langmuir*, 2014, **30**, 710–717.
46. V. garbin, J. C. Crocker and K. J. Stebe, *Langmuir*, 2012, **28**, 1663–1667.
47. V. garbin, i. Jenkins, T. Sinno, J. C. Crocker and K. J. Stebe, *Phys. Rev. Lett.*, 2015, **114**, 108301.
48. a. b. Subramaniam, m. abkarian, l. mahadevan and h. a. Stone, *Nature*, 2005, **438**, 930.
49. e. hermans, m. Saad bhamla, p. Kao, g. g. Fuller and J. Vermant, *Soft Matter*, 2015, **11**, 8048–8057.
50. p. erni, *Soft Matter*, 2011, **7**, 7586–7600.
51. S. Vandebril, a. Franck, g. g. Fuller, p. moldenaers and J. Vermant,
Rheol. Acta, 2009, **49**, 131–144.
52. m. pepicelli, T. Verwijlen, T. a. Tervoort and J. Vermant, *Soft Matter*, 2017, **13**, 5977–5990.
53. m. nagel, T. a. Tervoort and J. Vermant, *Adv. Colloid Interface Sci.*, 2017,
247, 33–51.
54. I. m. C. Sagis, *Appl. Rheol.*, 2010, **20**, 24380.
55. I. m. C. Sagis, *Rev. Mod. Phys.*, 2011, **83**, 1367–1403.
56. a. S. utada, a. Fernandez-nieves, h. a. Stone and D. a. Weitz, *Phys. Rev. Lett.*, 2007, **99**, 094502.
57. J. eggers and e. Villermaux, *Rep. Prog. Phys.*, 2008, **71**, 036601.
58. S. Tomotika, *Proc. R. Soc. London, Ser. A*, 1935, **150**, 322–337.
59. T. r. powers, D. Zhang, r. e. goldstein and h. a. Stone, *Phys. Fluids*, 1997, **10**, 1052–1057.
60. m. Tjahjadi, h. a. Stone and J. m. ottino, *J. Fluid Mech.*, 1992, **243**, 297–317.

61. X. liu, S. Shi, Y. li, J. Forth, D. Wang and T. p. russell, *Angew. Chem.*, 2017, **129**, 12768–12772.
62. J. F. revol, h. bradford, J. giasson, r. h. marchessault and D. g. gray, *Int. J. Biol. Macromol.*, 1992, **14**, 170–172.
63. S. homma, J. Koga, S. matsumoto, m. Song and g. Tryggvason, *Chem. Eng. Sci.*, 2006, **61**, 3986–3996.

64. J. Forth, X. liu, J. hasnain, a. Toor, K. miszta, S. Shi, p. I. geissler, T. emrick, b. a. helms and T. p. russell, *Adv. Mater.*, 2018, **30**, 1707603.
65. a. S. utada, e. lorenceau, D. r. link, p. D. Kaplan, h. a. Stone and D. a. Weitz, *Science*, 2005, **308**, 537–541.
66. S. Shi, X. liu, Y. li, X. Wu, D. Wang, J. Forth and T. p. russell, *Adv. Mater.*, 2018, **30**, 1705800.
67. m. Cui, T. emrick and T. p. russell, *Science*, 2013, **342**, 460–463.
68. X. liu, n. Kent, a. Ceballos, r. Streubel, Y. Jiang, Y. Chai, p. Y. Kim, J. Forth, F. hellman, S. Shi, D. Wang, b. a. helms, p. D. ashby, p. Fischer and T. p. russell, *Science*, 2019, **365**, 264–267.
69. W. Feng, Y. Chai, J. Forth, p. D. ashby, T. p. russell and b. a. helms, *Nat. Commun.*, 2019, **10**, 1095.
70. C. huang, J. Forth, W. Wang, K. hong, g. S. Smith, b. a. helms and T. p. russell, *Nat. Nanotechnol.*, 2017, **12**, 1060–1063.
71. D. Cai, p. S. Clegg, T. li, K. a. rumble and J. W. Tavacoli, *Soft Matter*, 2017, **13**, 4824–4829.
72. T. li, J. Klebes, J. Dobnikar and p. S. Clegg, *Chem. Commun.*, 2019, **55**, 5575–5578.
73. K. macmillan, J. r. royer, a. morozov, Y. m. Joshi, m. Cloitre and p. S. Clegg, *Langmuir*, 2019, **35**, 10927–10936.
74. F. ravera, e. Santini, g. loglio, m. Ferrari and l. liggieri, *J. Phys. Chem. B*, 2006, **110**, 19543–19551.
75. F. ravera, m. Ferrari, l. liggieri, g. loglio, e. Santini and a. Zanobini, *Colloids Surf., A*, 2008, **323**, 99–108.
76. a. mohraz, *Nat. Nanotechnol.*, 2017, **12**, 1021–1022.
77. m. n. lee, J. h. J. Thijssen, J. a. Witt, p. S. Clegg and a. mohraz, *Adv. Funct. Mater.*, 2013, **23**, 417–423.
78. D. Cai, F. h. richter, J. h. J. Thijssen, p. g. bruce and p. S. Clegg, *Mater. Horiz.*, 2018, **5**, 499–505.
79. K. n. pham, a. m. puertas, J. bergenholtz, S. u. egelhaaf, a. moussaïd, p. n. pusey, a. b. Schofield, m. e. Cates, m. Fuchs and W. C. K. poon, *Science*, 2002, **296**, 104–106.
80. D. bonn, h. Tanaka, g. Wegdam, h. Kellay and J. meunier, *Europhys. Lett.*, 1998, **45**, 52–57.
81. W. götze, *J. Phys.: Condens. Matter*, 1999, **11**, a1–a45. 82. C. a. angell, *Science*, 1995, **267**, 1924–1935.
83. p. Y. Kim, a. e. ribbe, T. p. russell and D. a. hoagland, *ACS Nano*, 2016, **10**, 6257–6264.
84. p. Y. Kim, a. D. Dinsmore, D. a. hoagland and T. p. russell, *Soft Matter*, 2018, **14**, 2131–2141.
85. h. Zheng, u. m. mirsaidov, l.-W. Wang and p. matsudaira, *Nano Lett.*, 2012, **12**, 5644–5648.

86. h. Zheng, r. K. Smith, Y. Jun, C. Kisielowski, u. Dahmen and a. p. alivisatos,
Science, 2009, **324**, 1309–1312.
87. e. r. Weeks, J. C. Crocker, a. C. levitt, a. Schofield and D. a. Weitz, *Sci- ence*, 2000, **287**, 627–631.

88. J. esquena, *Curr. Opin. Colloid Interface Sci.*, 2016, **25**, 109–119.
89. h. Cheung Shum, J. Varnell and D. a. Weitz, *Biomicrofluidics*, 2012, **6**, 012808.
90. h. Yuan, q. ma, Y. Song, m. Y. h. Tang, Y. K. Chan and h. C. Shum, *Mac- romol. Chem. Phys.*, 2017, **218**, 1600422.
91. q. ma, Y. Song, J. W. Kim, h. S. Choi and h. C. Shum, *ACS Macro Lett.*, 2016, **5**, 666–670.
92. m. inam, J. r. Jones, m. m. pérez-madrigal, m. C. arno, a. p. Dove and r.
K. o'reilly, *ACS Cent. Sci.*, 2018, **4**, 63–70.
93. S. D. hann, m. goulian, D. lee and K. J. Stebe, *Soft Matter*, 2015, **11**, 1733–1738.
94. S. D. hann, K. J. Stebe and D. lee, *ACS Appl. Mater. Interfaces*, 2017, **9**, 25023–25028.
95. S. D. hann, D. lee and K. J. Stebe, *Phys. Chem. Chem. Phys.*, 2017, **19**, 23825–23831.
96. S. D. hann, K. J. Stebe and D. lee, *Langmuir*, 2017, **33**, 10107–10117.
97. h. Tavana, a. Jovic, b. mosadegh, q. Y. lee, X. liu, K. e. luker, g. D. luker, S. J. Weiss and S. Takayama, *Nat. Mater.*, 2009, **8**, 736–741.
98. r. bian, r. lin, g. Wang, g. lu, W. Zhi, S. Xiang, T. Wang, p. S. Clegg, D. Cai and W. huang, *Nanoscale*, 2018, **10**, 3621–3625.
99. g. h. Koenderink, Z. Dogic, F. nakamura, p. m. bendix, F. C. macKintosh,
J. h. hartwig, T. p. Stossel and D. a. Weitz, *Proc. Natl. Acad. Sci. U. S. A.*, 2009, **106**, 15192–15197.
100. T. Sanchez, D. T. n. Chen, S. J. Decamp, m. heymann and Z. Dogic,
Nature, 2012, **491**, 431–434.
101. K.-T. Wu, J. b. hishamunda, D. T. n. Chen, S. J. DeCamp, Y.-W. Chang, a. Fernández-nieves, S. Fraden and Z. Dogic, *Science*, 2017, **355**, eaal1979.
102. F. C. Keber, e. loiseau, T. Sanchez, S. J. DeCamp, l. giomi, m. J. bowick, m. C. marchetti, Z. Dogic and a. r. bausch, *Science*, 2014, **345**, 1135–1139.
103. m. J. booth, V. restrepo Schild, S. J. box, h. bayley, V. r. Schild, S. J. box and h. bayley, *Sci. Rep.*, 2017, **7**, 9315.
104. g. Villar, a. J. heron and h. bayley, *Nat. Nanotechnol.*, 2011, **6**, 803–808.
105. m. a. holden, D. needham and h. bayley, *J. Am. Chem. Soc.*, 2007, **129**, 8650–8655.